Refurbishing Interference Filter External Cavity Diode Lasers for Cold Atom Experiments

Hannah Marie Buss

Bachelorarbeit in Physik
angefertigt im Institut für Angewandte Physik

vorgelegt der
Mathematisch-Naturwissenschaftlichen Fakultät
der
Rheinischen Friedrich-Wilhelms-Universität
Bonn

Mai 2024

Ich versichere, dass ich diese Arbeit selbstständig verfasst und keine anderen als die angegebenen Quellen und Hilfsmittel benutzt sowie die Zitate kenntlich gemacht habe.

Bonn, ...

Datum Unterschrift

1. Gutachter: Prof. Dr. Sebastian Hofferberth
2. Gutachter: Dr. Frank Vewinger

Contents

CHAPTER 1

Introduction

In atomic physics, single-mode lasers that have a narrow linewidth and a broad wavelength tunability find many applications. A relatively cheap solution for lasers that meet these requirements are semiconductor lasers with external cavities. A big advantage for these lasers is that they can be easily home built in an optics lab.

In 1981 a paper by M.W. Fleming and A. Mooradian was published presenting one of the first external cavity diode lasers (ECDL) [1]. In "Spectral characteristics of external-cavity controlled semiconductor lasers" the authors present a laser where a semiconductor as active gain medium is inserted into a double-ended cavity. The presented ECDL uses a diffraction grating in Littrow configuration as a tuning element. This means that a lens collimates the diode's output, which is then reflected by a diffraction grating that is used as the wavelength tuning element. This part effectively acts as the left side of the external cavity. The backreflection is then recollimated by a lens behind the diode and reflected by a mirror, creating the optical feedback in the right part of the external cavity. This mirror also acts as the outcoupler. Compared to semiconductor lasers that work without an external cavity, this configuration allows for more convenient wavelength tuning and variations to properties such as linewidth and threshold current [1].

Since this first publication, the development of ECDLs has shifted towards using single-ended external cavity lasers. This change is made by putting a reflective coating onto the backside of the diode, effectively placing the gain medium on one of the end mirrors. As this reduces the number of required optical elements, it increases stability and allows for a simpler alignment [2, p.369]. Most commercially available ECDLs today use this external cavity Littrow configuration, since they only require one antireflection coating operation on the diode while still offering excellent optical performance [2, p.368].

In the Littrow configuration ECDLs the position and angular orientation of the diffraction grating are very sensitive to mechanical vibrations and acoustic loads. This can cause fluctuations in both wavelength, power and output beam alignment [3]. A solution for this problem is presented in a paper by Baillard et al. from 2006 [4]. In this paper titled "Interference-filter-stabilized external-cavity diode lasers" an alternative ECDL design is proposed. Here, an interference filter is used as the frequency selective element, effectively separating the wavelength tuning and the creation of optical feedback to two different components. This new configuration makes it possible to adjust the feedback within the cavity using a partially reflective mirror, while independently tuning the wavelength by rotating an

interference filter that is inserted into the cavity. With this, interference filter ECDLs are much more insensitive to mechanical effects, making them a great design to build in the lab.

Most of the lasers used within the Nonlinear Quantum Optics Group in Bonn are Toptica DL pro lasers, commercial ECDLs that use the Littrow configuration. For my thesis in this group, an alternative to them is created. Two already existing interference filter ECDLs that were originally made to lase at a wavelength of 852 nm are being refurbished to use in the Rubidium Quantum Optics experiment (RQO). The new wavelength for both lasers is 780 nm, the wavelength corresponding to the D2 line in the Rubidium spectrum. To refurbish the lasers, their laserdiodes and interference filters have to be exchanged to components made for this wavelength. All other elements can be reused as they are broadband for the near infrared spectral range.

A second goal for this thesis is to work with the existing design for these lasers and the manual for building them. The thesis aims to allow later students to look up steps of setting up the optical and mechanical parts of the ECDLs.

Chapter 2 gives a short introduction into ECDL designs. In chapter 3, the individual components for building an interference filter ECDL and its assembly are explained. The working lasers are then characterized in terms of current-power-wavelength correlation, beamprofile, and wavelength stability in chapter 4. Finally, in chapter 5, the lasers are used to perform Rubidium spectroscopy and a current feedforward is implemented next to the frequency scan via piezo element.

CHAPTER 2

External Cavity Diode Lasers

This thesis focuses on semiconductor lasers with an external cavity. These lasers use laserdiodes as their gain medium, which are incorporated in external cavities with variable lengths to achieve narrower linewidths and frequency tunability. A common configuration of these external cavity diode lasers (ECDL) is the so-called Littrow configuration (see Figure 2.1(a)) where a reflection grating is used to tune the laser in wavelength [2, p.387]. A different approach that is much more insensitive to mechanical and thermal disturbances is a design where instead of the grating, an interference filter (IF) is inserted in the external cavity to tune the laser's wavelength, as shown in Figure 2.1(b) [4]. This design is commonly referred to as interference filter ECDL or IFL for short.

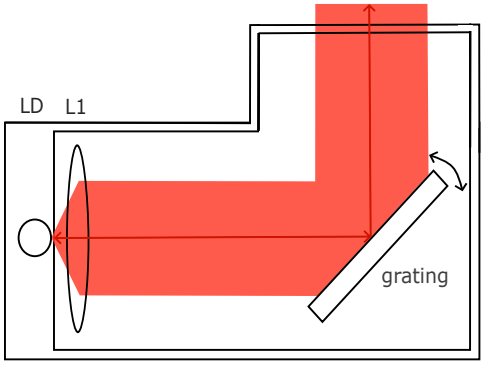

(a) ECDL in simple Littrow configuration. The output of the laser diode LD is collimated by lens L1. The beam hits the diffraction grating, where the first order diffraction is reflected at the incidental angle and the zeroth order diffraction is reflected as the output beam. By rotating the grating, the wavelength is tuned.

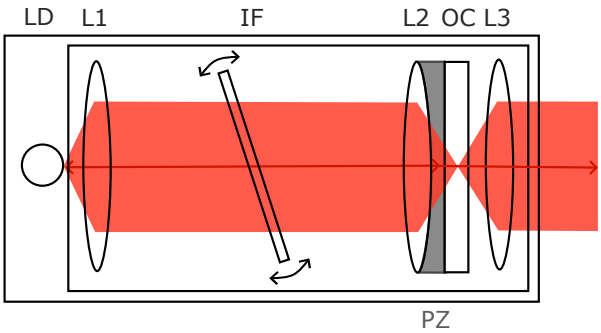

(b) IF-ECDL with configuration as used for this thesis. The laser diode's (LD) output is collimated by lens L1. It passes through the tuning filter IF and is focused onto the half mirror OC by L2. OC both creates optical feedback and acts as an outcoupler. The wavelength can be tuned both by rotating IF and using a piezoelectric actuator PZ. The output beam is recollimated by lens L3.

Figure 2.1: Schematic diagram of two configurations of ECDL

The most popular version of ECDLs uses the same optical element for creating optical feedback and tuning the wavelength. A sketch of this so-called *Littrow configuration* can be seen in Figure 2.1(a). Here, the diffraction grating is aligned in such a way that the first diffraction order is reflected back with

the incidental angle so that it couples back into the laser [5]. Its zeroth order diffraction is reflected as the output beam. The wavelength that is both reflected back at exactly the incidental angle and diffracted at the desired output angle depends on the angular orientation of the grating.

One of the disadvantages that come with this configuration is that tuning the wavelength by rotating the grating displaces the output beam [6]. This can be counteracted by adding a second mirror into the beampath that corrects this angular displacement by rotating it accordingly. Another problem that comes with this configuration is mode hopping as the wavelength is tuned [5]. There are multiple well known configurations that circumvent both of these problems by using separate optical elements for creating optical feedback and tuning the wavelength, such as the Littman-Metcalf configuration which is further explained in [7], and the IFL that is being used here.

The IFL configuration consists of an external cavity in which a wavelength tuning element is inserted. The output of the laserdiode is collimated using a lens with a short focal length and a high numerical aperture. At the end of the cavity, a partially reflecting mirror acts as an outcoupler for the output beam and creates the optical feedback. This mirror is part of a *cat eye construction* made up of the outcoupling mirror and a lens which provides higher stability against misalignment [4]. The mirror is mounted on a piezoelectric actuator (PZ) as a way to vary the cavity length and thereby the laser's wavelength. The cat eye lens focuses the collimated beam onto the outcoupling mirror that is mounted on PZ.

An interference filter is inserted into the collimated beam inside the cavity. It is important that the light passing through this filter is collimated to ensure that its functionality is as expected [8].
To understand the wavelength tuning in this configuration, a closer look at the interference filter is taken. The simplest type of these filters are Fabry-Perot etalons with a thickness $d \sim \lambda$. They are made of a thin glass substrate with two highly reflective coatings on either side. These coatings are usually made from dielectric stack mirrors, which gives the filter a narrow transmission peak [2, p.392]. In modern interference filters, a peak-width of below 2 nm and a maximum transmission of 90 % can be reached [9, p.162].
The wavelength with maximum transmission through the etalon λ_{max} depends on the angle of incidence θ [4]:

$$\lambda_{\text{max}} = \lambda_{90^\circ} \cdot \sqrt{1 - \frac{\sin^2 \theta}{n_{\text{eff}}^2}} \,. \tag{2.1}$$

Here n_{eff} is the effective refractive index of the filter and λ_{90° the wavelength at normal incidence.

The filter that is used for these lasers usually has a linewidth similar to that of the cavity. By inserting it inside the cavity however, its broader filtering effect is amplified quite strongly, which leads to a narrow linewidth of the output beam.

CHAPTER 3

Building an Interference Filter Laser

In this chapter it is explained how the individual parts of the two lasers, IFL004 and IFL005, are assembled, starting with the temperature control in subsection 3.1.1 and then continuing with the assembly of the inner housing, which is the part that I have done myself to refurbish the two lasers. Here the laser diode and its collimation tube are installed in subsection 3.1.2, the interference filter is added to the housing in subsection 3.1.3 and the cat eye construction is built. It is then used to close the cavity in subsection 3.1.4.

With the laser being built there are a couple of changes made to some parts to adjust certain laser characteristics such as the Polarization (subsection 3.2.1), the threshold (subsection 3.2.2) and the wavelength (subsection 3.2.3).

3.1 Assembly

The lasers are built into an aluminium housing that has been made by the mechanics workshop of the Institute of applied physics. It consists of an outer housing in which the electronics and temperature controlling elements are placed, and an inner housing that is fixed on top of the former, which houses the optical elements. A technical sketch of these housings can be seen in Figure 3.1. A schematic of the configuration inside of the inner housing is shown in Figure 2.1(b). The laser can be fixed on the table using the screw holes at the bottom of the outer housing. To ensure more thermal and sound isolation, one can add an isolating material to the inside of the outer housing.

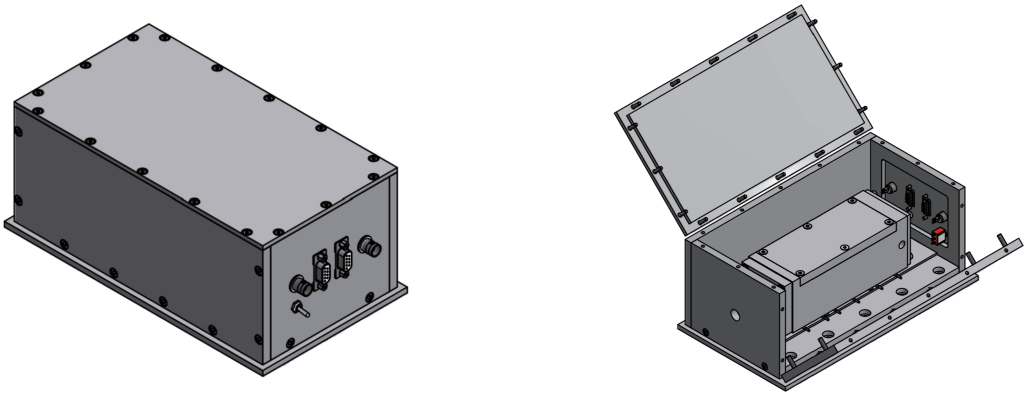

Figure 3.1: Technical sketches of the inner and outer housing for the self built laser

3.1.1 Temperature Control

To control the diode temperature of the laser, three Peltier elements[1] are connected in series and then placed on the indentations on the ground plate of the outer housing, which is shown in Figure 3.2(a).

A thin film of thermal heatsink paste is spread out both on the ground plate indentations and on top of the Peltier elements. After this, the inner housing is placed on top of the Peltier elements and screwed in place with six nylon screws (M6) which make sure that the housings are thermally isolated from each other. It is important that during this step, a bolt nut (M4) is placed in the hole at the bottom of the inner housing so that the interference filter can be fixed to it later on. After installing the inner housing, the two outermost cables from the Peltier elements are soldered to pins 4(+) and 5(-) of the connector at the back wall of the outer housing. It is connected to the temperature control as shown in Figure 3.3.

After this, the temperature sensor is mounted in the inner housing. The placement is chosen close to the space for the diode. Here either an AD590 or an NTC 10K 3625K can be used. Both lasers that were refurbished for this thesis use an AD590 due to the fact that for this type of sensor, the temperature display on the control unit is in °C. This is more convenient than the display for the NTC sensor, which is giving out a resistance in Ω. The AD590 is glued into the bigger hole left of the hole for the collimation tube using thermal heatsink glue, the NTC sensor is glued into the smaller hole on the right of the collimation tube, which can be seen in Figure 3.2(b). The glue needs to fully connect the sensor and the housing to ensure good thermal contact. After this, the sensor is soldered to the temperature control connector according to Figure 3.3. The controller that is used is a Thorlabs ITC102 controller, a combined current controller and thermoelectric cooler, that has a maximum laser current of 200 mA.

[1] Standard Peltier-Element 12705 40x40x4mm Nominal voltage 15.4 V

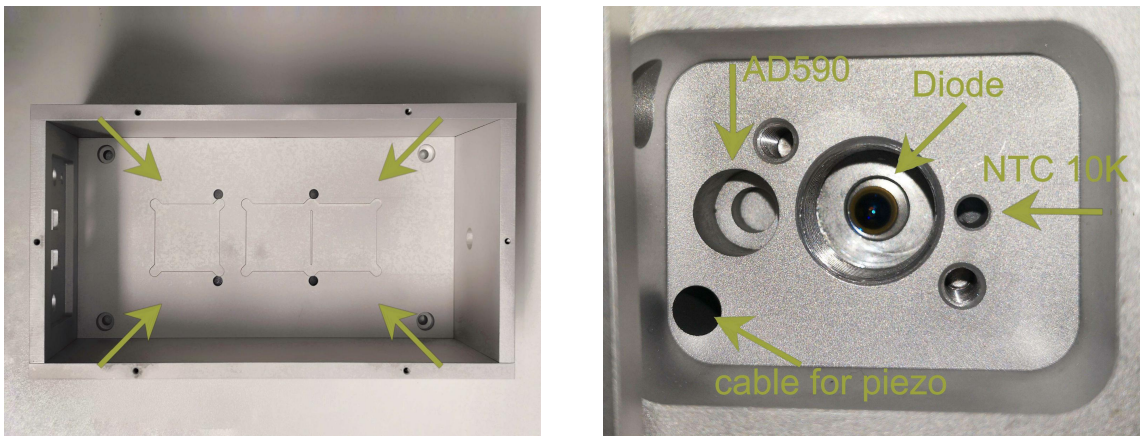

(a) Outer housing with three indentations to place Peltier elements that are used for temperature stabilization of the inner housing.

(b) Open backpanel of the inner housing with spaces for temperature sensors

Figure 3.2: Spaces for the peltier elements and temperature sensors in the outer housing and back of the inner housing

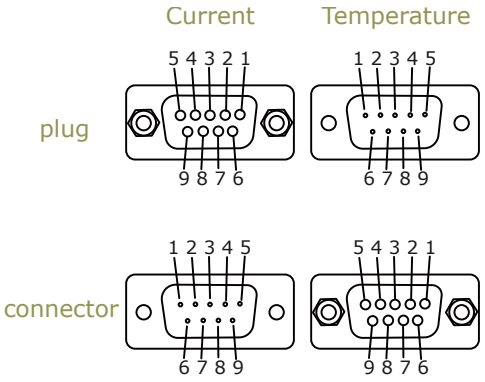

Figure 3.3: Pin layout for the connectors at the back of the outer housing and plugs

Pin assignment	9 pin connector pin	
	Current (f)	Temperature (m)
Interlock (< 430Ω to Interlock GND)	1	
PD cathode in	2	
LD ground	3	
PD anode in	4	
Interlock GND	5	
AD590 +		9
TEC +		4
TEC -		5
Bias - out (should be disabled by JP2)	6	
LD cathode out (polarity AG)	7	
LD anode out (polarity CG)	8	
Bias + out (should be disabled by JP1)	9	
AD590 -		7
Thermistor GND		3
Thermistor		2

Table 3.1: Pin Assignments

Figure 3.4: Pin connections for temperature and current control

3.1.2 Laser Diode and Collimator tube

Collimating the Laser Diode

(a) Diode glued on retaining ring.

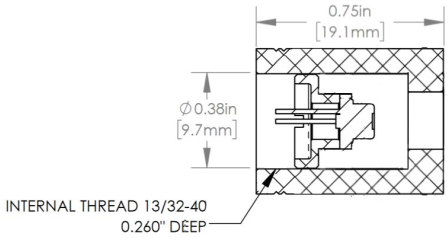

(b) Collimation tube sketch, modified from Thorlabs spec sheet [10]. The diode and the retaining ring are inserted halfway into the tube.

Figure 3.5: First collimation tube solution

After mounting the inner housing, the diode is installed in the back part (see Figure 3.2(b)) of the inner housing along with an aspherical lens to collimate its light (L1). Depending on the thread in the hole for the collimator tube, this is done a little differently. With the configuration that is given here, the diode is fixed in the collimation tube by a retaining ring that is screwed in behind it. There are two different sizes of diodes that can be used for this laser: in the previous version a Ø9 mm package diode was used which fits in the used collimation tube when the retaining ring is used. For the refurbished lasers, a Ø5.6 mm package diode[2] is used. Since this diode is smaller than the diameter of the tube some sort of adapter is needed. There is an adapter ring that can be used to position the diode at the center of the tube but since it also adds to the height of the diode construction, it makes it impossible to collimate the diodes output in the given constellation.

The easiest solution to mount the diode in this constellation is to glue it onto the retaining ring as shown in Figure 3.5(a) and thereby also ensuring its position in the center of the tube while not adding to its height. In this version, the lens used to collimate the diode's output (L1) is mounted in an aluminium plate that is screwed to the inside of the inner housing by two screws. This allows for more freedom when adjusting the position of the lens than in the constellation described below.

An alternative solution to be able to mount both sizes of diodes is using a Thorlabs collimation tube[3] that has a narrower part which corresponds to the focal length of the used aspherical lens for easier collimation. A sketch of the tube is shown in Figure 3.6. This is the tube that the retaining ring and diode adapter used in the first option were originally designed for, which means the added diode height does

[2] Thorlabs diode type L785P090
[3] Thorlabs tube type LT230P-B

(a) Collimation tube with inserted diode.

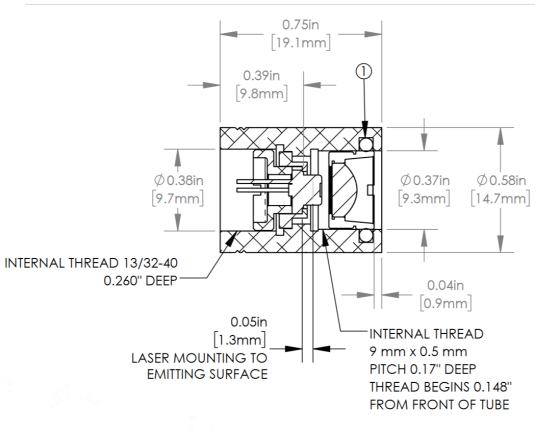

(b) Collimation tube sketch from Thorlabs spec sheet [10], showing the diode mounted in the collimation tube using a retaining ring and adapter. The collimation lens is also mounted in the front.

Figure 3.6: Second collimation tube solution

not affect the collimation of its light. In this constellation, L1 is mounted in the collimation tube, where its position along the z-axis can still be adjusted. The possibility to move it in the x- and y-direction, which is given in the previous solution, is not available here.

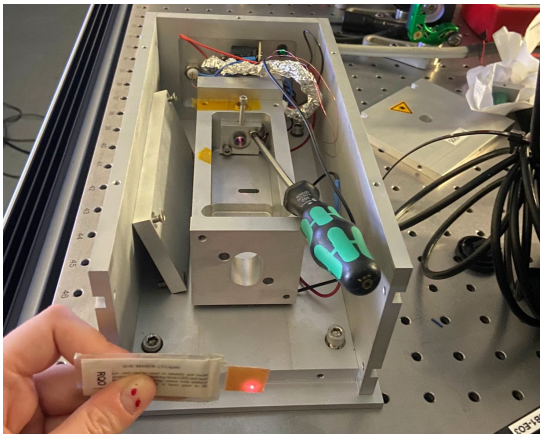

(a) Collimation by eye

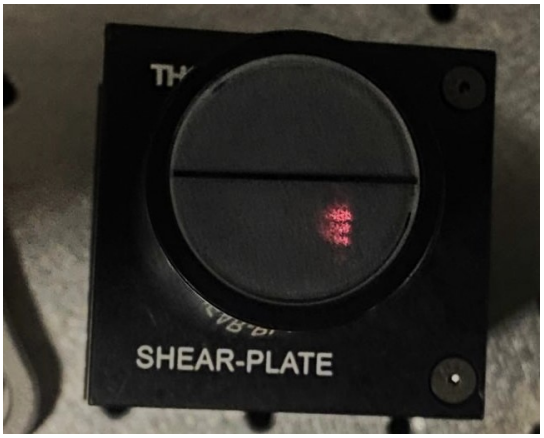

(b) Shearplate interferometer showing a collimated beam

Figure 3.7: Collimating the laser diodes output

Since both lasers that have been refurbished for this work came with a collimation tube of the first type, the collimation lens L1 has to be mounted separately from the diode and collimation tube. After installing the diode in the collimation tube, L1[4] is screwed into the aluminium holder. The holder is then screwed to the inner housing using two M4 screws with washers (for easier position adjustment) after

[4] Thorlabs lens type A230TM-B

which the lens position along the z-axis is adjusted by screwing/unscrewing it using a spanner wrench[5]. Both collimation processes that were used are shown in Figure 3.7. The collimation is first checked by eye. For this, the beam size is checked at different distances using a detection card that is held into the beam. To check it at longer distances, a mirror is added into the beam to reduce the space needed for this. A more precise collimation can be achieved by putting a shear plate interferometer into the beam. The beam hits a glass plate and is reflected both on its front and back surface. These two reflections are overlapped on a diffuser plate, where the interference between them is visible through an IR-viewer or a similar device. If the interference fringes are aligned with the line on the plate, the beam is collimated. If they are at an angle compared to it, the beam is either convergent or divergent.

After the output of the laser diode has been collimated, the position of the aluminium holder with L1 is adjusted so that the output beam is straight and at a height of 5 cm which is the height of the main experiment in the RQO lab. This is done by screwing a longer M4 screw into the top of the holder and slightly unscrewing the two screws holding it in place. The aluminium plate can then be moved around until the beam is at the desired position on a beam blocker as far away from the laser as possible as seen in Figure 3.8[6]. The diode is now done being installed. Its position will be adjusted a bit to set the polarization in subsection 3.2.1. It is also possible to set the polarization before continuing the assembly to ensure the output beam does not change after the assembly is done.

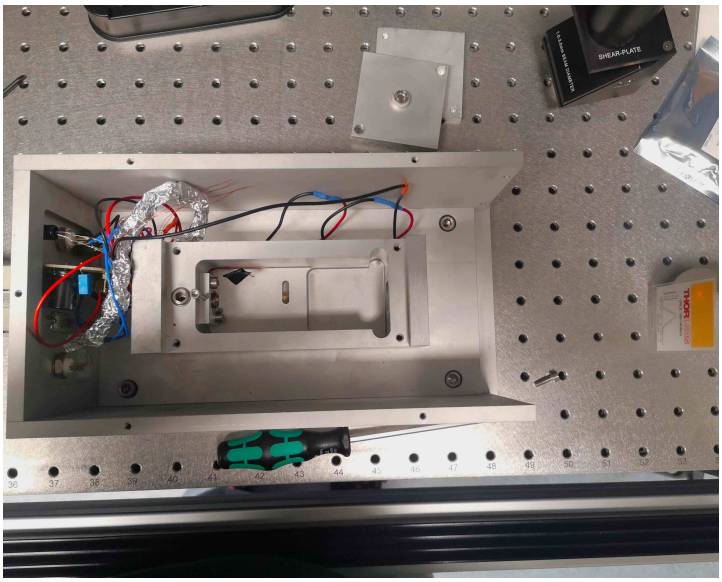

Figure 3.8: Adjusting the angle of the collimated diode output emission.

Characterizing the diode

For both lasers that were refurbished for this thesis, the threshold of the diode (see Figure 3.9) and the wavelength as a function of temperature (see Figure 3.10) were measured.

[5] Thorlabs tool type SPW301

[6] On this photo the beam blocker has been placed closer to the laser for better visualization of the progress.

Since the external cavity is supposed to lower the threshold compared to that of the base laser diode, it is useful to measure this before continuing the assembly of the laser by putting a powermeter into the beam and measuring the output for increasing currents.

When fitting a linear function[7] to the part with a linear increase in power, that shows the diode is lasing, the following values for the lasing thresholds can be obtained:

$$I_{\text{thr 004}} = (26.63 \pm 0.22)\,\text{mA} \tag{3.1}$$

$$I_{\text{thr 005}} = (28.35 \pm 0.22)\,\text{mA}. \tag{3.2}$$

The curve for IFL004 was recorded at a diode temperature of 20.0 °C, the one for the diode in IFL005 at a temperature of 23.6 °C. Comparing this to the value given for a temperature of 25.0 °C by the manufacturer Thorlabs, who puts the typical threshold current to $I_{\text{thr TL}} = 35$ mA, this is already relatively low.

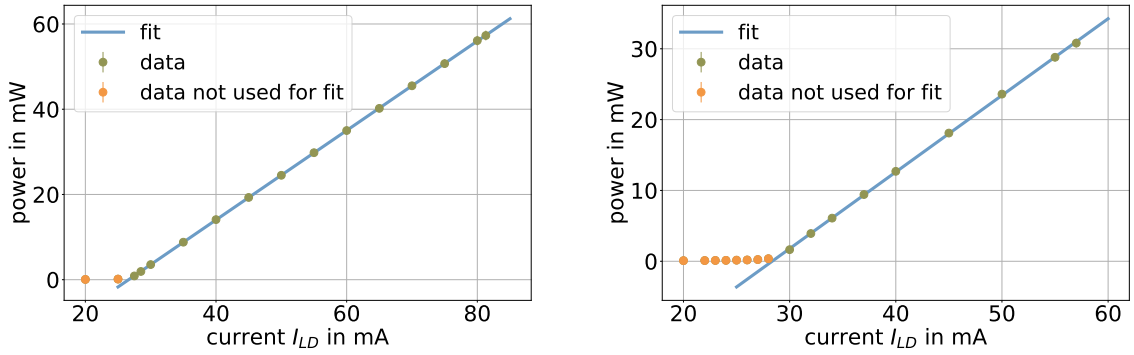

(a) Laser diode used in IFL004, measured with a diode temperature of 20 °C. The lasing threshold is at (26.63±0.22) mA. The errorbars are too small to be visible.

(b) Laser diode used in IFL005, measured with a diode temperature of 23.6 °C. The lasing threshold is at (28.35±0.22) mA. The errorbars for the measured values are too small to be visible.

Figure 3.9: Lasing threshold measurements for the used laser diodes.

To measure the wavelength dependency on the temperature, the output is coupled into a multimode fiber that is connected to a wavemeter[8]. The diode temperature is then slowly increased using the laser controller. Here, it is important to wait until the temperature has set before measuring the wavelength, since the temperature control's PID circuit sometimes takes a while to settle on the correct temperature. The temperature range for which this measurement is done is between 17 °C and 26 °C since the peak wavelength 785 nm that is given by Thorlabs corresponds to a temperature of 25 °C. To get the wavelength of this laser to be smaller than the given value, it makes sense to go to lower temperatures. The measurement is taken to find the mode hop-free tuning range that is given by temperature changes.

The plots for the wavelength as function of diode temperature look relatively similar for both of the

[7] All the linear fits done for this thesis are calculated using orthogonal distance regression.

[8] Wavelength Meter Ångstrom WLM-VIS High Finesse WS7

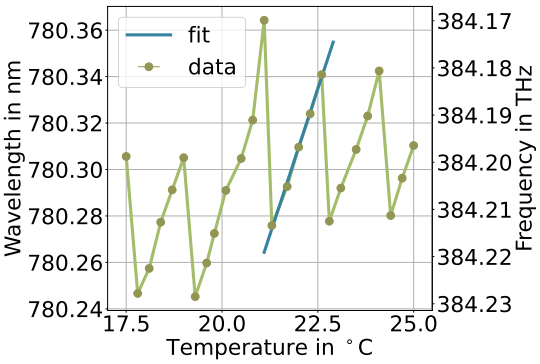

(a) Laser diode used in IFL004, measured with a diode current of 32 mA. The errorbars are too small to be visible.

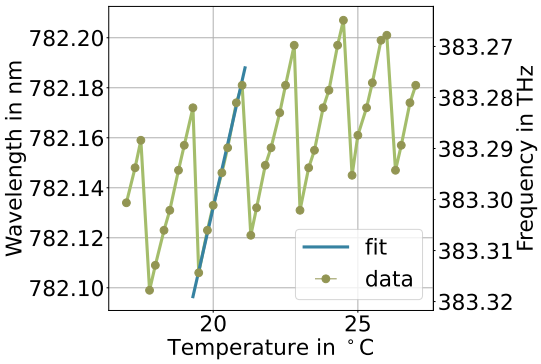

(b) Laser diode used in IFL005, measured with a diode current of 28.8 mA. The errorbars are too small to be visible.

Figure 3.10: Temperature-Wavelength measurements for the used laser diodes. The linear slope is characteristic for a standalone laserdiode. The sudden jumps in the measurement are mode hops.

diodes, the tuning range is slightly larger for the diode used in IFL005:

$$\Delta\nu_{\text{temp 004}} = (73.991 \pm 0.063) \times 10^{-3}\,\text{nm} \mathrel{\widehat{=}} (36.431193 \pm 0.000015)\,\text{GHz} \tag{3.3}$$

$$\Delta\nu_{\text{temp 005}} = (71.200 \pm 0.010) \times 10^{-3}\,\text{nm} \mathrel{\widehat{=}} (34.8911083 \pm 0.0000025)\,\text{GHz}. \tag{3.4}$$

This is determined by subtracting the smallest wavelength from the largest between two mode hops and then averaging over all the tuning ranges that were measured.
The tuning slopes within these ranges are

$$\left(\frac{\Delta\lambda}{\Delta I}\right)_{\text{temp 004}} = (50.3 \pm 1.6) \times 10^{-3}\,\text{nm/°C} \mathrel{\widehat{=}} (24.76 \pm 0.76)\,\text{GHz/°C} \tag{3.5}$$

$$\left(\frac{\Delta\lambda}{\Delta I}\right)_{\text{temp 005}} = (50.8 \pm 1.4) \times 10^{-3}\,\text{nm/°C} \mathrel{\widehat{=}} (25.05 \pm 0.66)\,\text{GHz/°C}. \tag{3.6}$$

This has been determined by assuming the slopes are the same for all tuning ranges and then fitting a linear function to one of them, which is shown in Figure 3.10. Both of these characteristics can later be used to finetune the wavelength in case the desired wavelength is skipped by a mode jump when tuning with the interference filter as described in subsection 3.2.3.

3.1.3 Interference Filter

After the diode has been characterized, the interference filter is inserted into the cavity as a frequency selective element. First, The filter first to be glued into a holder so that it can then be fixed into a kinematic mount. Before glueing it into the holder, it is important to check that the filter is clean. Since the filter is rather small, any dirt on it can cause significant impairments to the quality of the cavity. Once it is clean, the filter can be glued into the holder, which is a small aluminium ring that has been homemade by the workshop specifically for this purpose. This is done by placing four small dots of glue, either two component glue or superglue can be used, 90° apart on the indentation on the front side of the

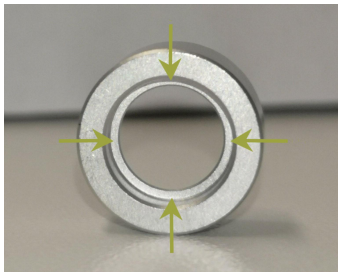

(a) Glue placement on the aluminium holder

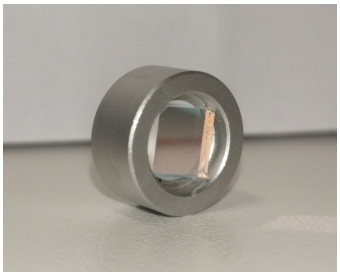

(b) Filter glued in the holder

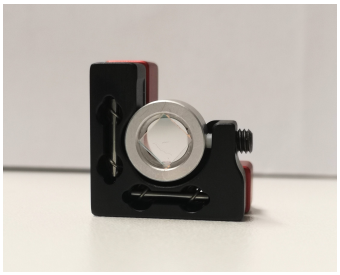

(c) Filter with holder in mechanical mount

Figure 3.11: Mounting process for the interference filter

ring (see Figure 3.11(a)). The filter is placed in the ring in a way that none of its edges touch the glue and then rotated so all four corners are aligned with the glue dots. Glueing the filter in this way ensures that a minimal amount of glue is on the filter. If necessary the filter can be pressed down using a wipe and gloves so that it sits perfectly straight in the holder (see Figure 3.11(b)).

Once the glue is hardened, the aluminium ring can be mounted in a mechanical mount[9]. This kinematic mount allows one to fine tune the filter's angle later on by turning its screws. It is important to orientate the filter as it is shown in Figure 3.11(c), since the beam in the cavity can be rather wide. By aligning the filter angle this way, the maximum amount of light is transmitted.

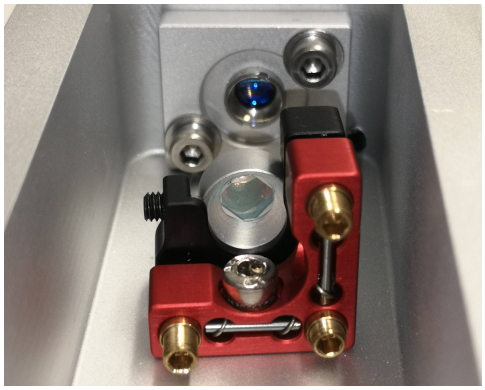

(a) Placement of the mounted interference filter inside of the inner laser housing.

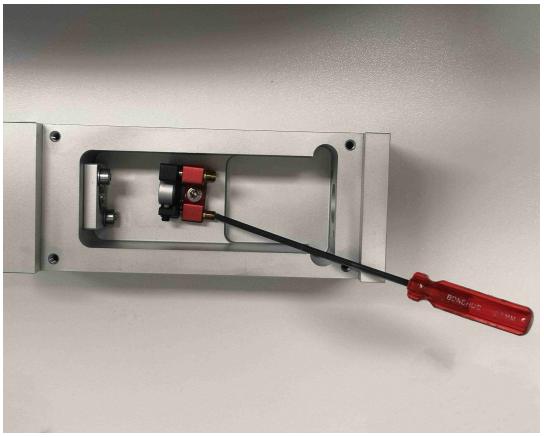

(b) View of the filter placement in the inner housing from above, showing the screw accessibility for wavelength tuning.

Figure 3.12: Installing the mounted filter in the inner housing of the laser

The mounted filter is then placed into the inner housing. Using an M4 22 mm screw, the mount is screwed to the base of the inner housing using the bolt nut that was placed under the slit in the baseplate in subsection 3.1.1. It is recommended to place the mount in a way such that the filter faces the diode. This allows for easier access of the adjustment screws to later tune the wavelength using the angle of the filter with respect to the beam path. Once the filter is placed, it is carefully rotated by hand until the

[9] MINI-H-U-3-3030, Radiant Dyes

angle of maximum transmission is reached and then screwed down tightly. This is done for convenience, since more transmission makes the rest of the assembly a lot easier. The tuning to the desired wavelength is done after the assembly, described in subsection 3.2.3.

The filter that is used in both of the lasers is an interference filter from Radiant dyes for 780 nm. This wavelength is transmitted at an angle of 6° and has a tuning range of up to 20 nm (from 761 nm to 783 nm). According to the Radiant dyes website the filter has a transmission of over 90% for different wavelengths and a linewidth of $\Delta\lambda_{\mathrm{FWHM}} = 0.37\,\mathrm{nm}$.

Since these characteristics given by the manufacturer are only approximations that differ from batch to batch of produced filters, I measured the transmission as a function of filter angle for a wavelength of 780.238 nm. The measurement is taken by placing the filter into the output beam and recording the transmitted power with a powermeter. The result of this measurement can be seen in Figure 3.13. It is done by noting down the number of screw turns for each power measurement, and then later converting the screw turns to a filter angle by measuring the filter's dimensions and finding the 0°-angle by looking at the backreflection from the filter.

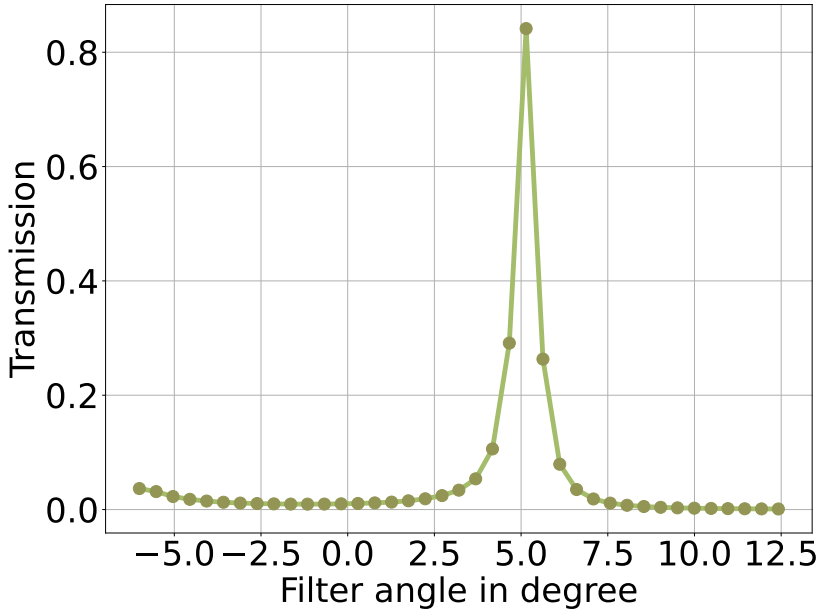

Figure 3.13: Transmission through the used interference filter for different angles. The transmission was measured for a wavelength of 780.238 nm. The filter angle has an uncertainty of approximately 0.1° which is too small to be visible in this plot.

3.1.4 Cat eye construction

With the gain medium and the filter being installed, the cavity can now be closed. For that, a cat eye construction is built by glueing a ring piezo and a mirror on an aluminium plate.

First the piezo[10] is glued on the aluminium plate using a thin film of two component glue. The piezo

[10] HPSt150/14-10/12, Piezomechanik

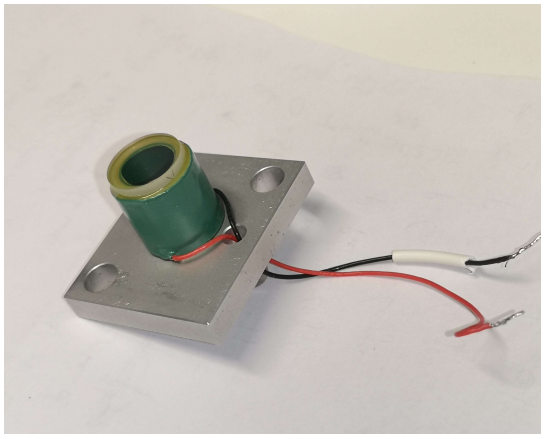

(a) Piezo and outcoupler mirror glued to the aluminium plate

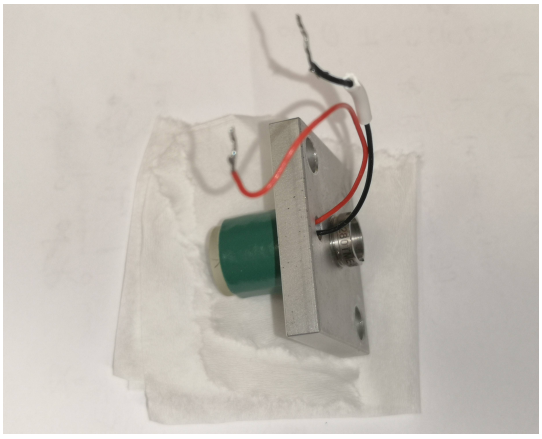

(b) Piezo/outcoupler with cat eye lens (L2) installed in aluminium plate

Figure 3.14: Assembled outcoupling mirror part before being put into the laser.

cables can then be fed through the top hole of the plate as shown in Figure 3.14(a). It might be more convenient to do this before glueing the piezo in place. Once the glue has hardened, the outcoupler mirror[11] is placed on the piezo with the reflective side facing the piezo. This mirror is the component that determines the strength of the optical feedback in the cavity. By choosing higher reflectivity mirrors, the optical feedback is increased while the output intensity is decreased. The used mirror has been chosen according to this.

After checking that the mirror is facing the right way, a thin film of glue is applied to the piezo and the mirror is added on top of it. The cat eye lens (L2)[12] is then screwed into the thread of the aluminium plate to finish the outcoupling mirror part. The finished part can be seen in Figure 3.14(b).

The construction is then installed in the inner housing by carefully inserting the piezo/mirror part into the tube in the frontplate and screwing the aluminium plate to it with two (M4) screws. Here, just like with L1 (see subsubsection 3.1.2), it is useful to add washers under the screws to make the laser resonator adjustment in subsection 3.2.2 easier. This makes the plate less likely to move when screwing the screws more tightly.

Since the first cat eye lens (L2) refocuses the laserbeam, another lens L3[13] is added outside the cavity to recollimate it. It is screwed into an aluminium plate that is then screwed to the front of the inner housing as shown in Figure 3.15.

This lens is used to collimate the beam output by adjusting its position along the propagation axis, which can be checked either by eye or with a shear plate interferometer as it was done in subsubsection 3.1.2. The angle of the output beam can be changed by changing the x- and y- position of the aluminium plate. The output beam of the two lasers I have worked with is orthogonal to the laser housing and has a height of 5 cm.

[11] Mountain Photonics, Q4.2011, Transmittance = 68.1 % at 852 nm, AOI=0°

[12] Thorlabs lens type A280TM-B

[13] Thorlabs lens type C560TME-B

Figure 3.15: Holding plate for the recollimation lens (L3) at the front of the laser's inner housing. L3 is not placed yet. In the back, the first collimation lens L1 of the laser diode is visible.

Once these steps are complete, the laser is done being assembled. Ideally, it should now have a collimated output beam. If this is not the case, the positions of the outcoupling part and L3 can be adjusted. This is done by slightly unscrewing the two screws fixing either plate to the housing and moving the aluminium plate with a longer M4 screw that is inserted in the plate for better control. This process is repeated until an output is visible which is the basis for aligning it for optimal performance in the next step, described in section 3.2. Another thing that might need to be adjusted before the laser works and can be optimized, is the z-position of L2, which is done by screwing it deeper (or unscrewing it) into the aluminium plate using the spanner wrench that was also used to collimate the diode's light in subsubsection 3.1.2.

In order to use the piezo for scanning, the cables that are inside of the inner housing need to be connected to two other cables that are inserted in the cavity from the back end. It is recommended to use longer cables for this in order not to have to solder inside the inner housing. The cables can be seen in the photo of the finished laser in Figure 3.16. The connecting cables are then connected to the BNC-connector at the backpanel of the outer housing.

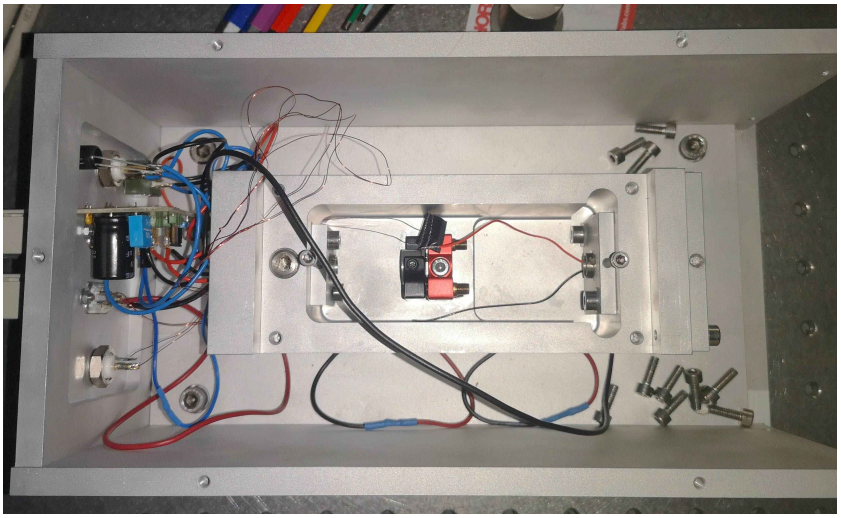

Figure 3.16: The finished laser with open inner housing. The collimation lens can be seen on the left side of the inner housing, as well as the IF in the middle and the cat eye lens on the right.

3.2 Adjustments

Now that the laser is done being built, some adjustments are made to some of its characteristics. Here, setting the polarization of the laser beam and adjusting the resonator are adjustments to be made once after building the laser and then not touching them again. The interference filter can be adjusted more easily once everything else is done, and it is no problem to tune the laser's wavelength even after it has been in use for some time.

3.2.1 Set Polarization

Since the diode emits polarized light, the polarization can be changed by rotating the diode. To do so, the back panel of the laser has to be opened and the diode is unplugged. It can then be rotated in the collimation tube with the spanner wrench that was also used to screw the lenses into the aluminium plates. This also slightly changes its position along the z-axis. It is possible that after this the collimation might have to be slightly adjusted.

The easiest way to measure the polarization is to use a rotable polarization beamsplitter (PBS), rotate it such that the desired polarization is completely reflected, and then adjust the diode's orientation until the power measured behind the PBS reaches a minimum. This setup can later also be used to determine both the exact polarization by determining the angular orientation at which the maximum amount of power is transmitted, and the polarization extinction ratio (PXR) by measuring the minimal and maximal transmissions. The PXR is then calculated as

$$\mathrm{PXR} = -10 \log \frac{P_{\mathrm{min}}}{P_{\mathrm{max}}}. \tag{3.7}$$

One problem that occurred when setting the polarization was that because the retaining ring for the diode sits rather loosely inside the collimation tube, the orientation of the diode sometimes changes

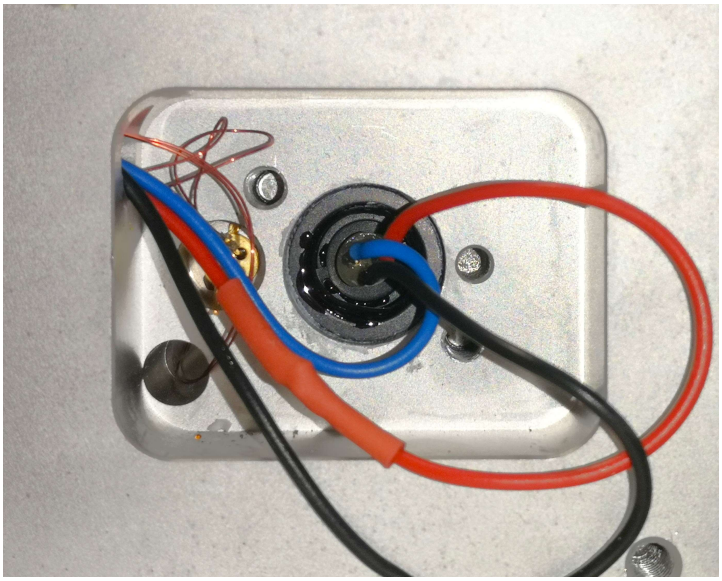

Figure 3.17: Opened backpanel with glued in diode after the polarization has been adjusted

when the cables connected to it are touched. Since these cables are fed through a hole at the side of the inner housing and connected to the outer housing's back panel this happens rather often. It even occurred when the back panel was closed and the aluminium plate touched the cables. To avoid this, the diode was glued into the collimation tube after setting the polarization using a small drop of two component glue as shown in Figure 3.17. In addition to this, a piece of tissue (more ideally a piece of foam could be used) was added to the feed through hole to minimize movement of the cables after closing the back of the inner housing. The combination of both of these things was enough to make sure the polarization stayed constant, but this still made the process of setting the polarization much harder.

After these adjustments, the polarization was measured: IFL004 has a horizontal polarization of 1°. It has a PXR of 19.89 dB. The second laser, IFL005, has an approximately vertical polarization (90°) and a PXR of 15.4 dB.

3.2.2 Laser Resonator Adjustment

As the final optimization, the resonator is adjusted in order to lower the lasing threshold as much as possible. For this a longer screw is inserted into the aluminium plate that holds the cat eye construction and the two screws fixing it to the housing are unscrewed a bit.

To adjust the resonator, the diode current is set to a point that is slightly below the threshold - this can be seen by looking at the output on a detector card while gradually lowering the current. Once the spot on the detector card suddenly gets much more dim, the lasing threshold has been crossed. At this point, the position of cat eye construction can be adjusted until the spot on the detector card is bright again. This process is iteratively repeated until it is no longer possible to get the laser to lase below the previous threshold current. Once the lowest possible threshold is reached, a power curve as a function of diode current can be measured to precisely determine the lasing threshold. The threshold curves that have been measured for the lasers that have been refurbished here can be seen in Figure 3.18. From them, the

threshold currents can be determined to be at

$$I_{\text{thr 004}} = (24.37 \pm 0.72)\,\text{mA} \tag{3.8}$$
$$I_{\text{thr 005}} = (27.02 \pm 0.82)\,\text{mA}. \tag{3.9}$$

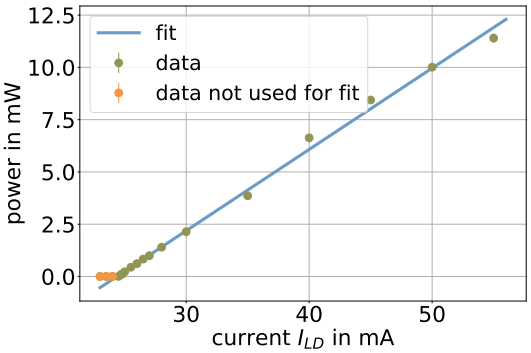

(a) Measurement for IFL004 at a diode temperature of 17.3 °C. The lasing threshold is at (24.37±0.72) mA. The errorbars are too small to be visible.

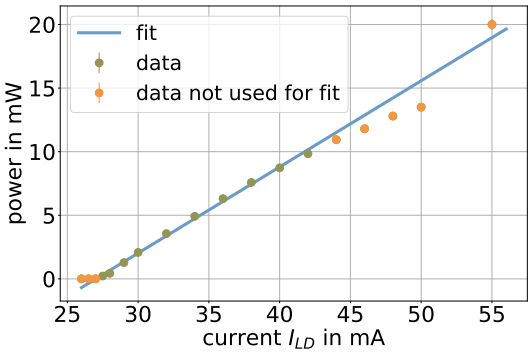

(b) Measurement for IFL005 at a diode temperature of 24.0 °C. The lasing threshold is at (27.02±0.82) mA. The errorbars are too small to be visible.

Figure 3.18: Lasing threshold measurements for both lasers after the resonator adjustments

Comparing this to Equation 3.1 one can see that the lasing thresholds have been lowered compared to those of the diodes on their own.

3.2.3 Internal Interference Filter Adjustment

The finished laser can now be tuned to different wavelengths by changing the angle of the interference filter inside of the external cavity. This is done by turning the lower outer screw of the filter mount with a 2 mm hex key and monitoring the wavelength on the wavemeter. The filters in the two lasers allow for a tuning range of approximately

$$\Delta\lambda_{\text{filter 004}} = 2.29\,\text{nm} \mathrel{\widehat{=}} 1.12\,\text{THz} \tag{3.10}$$
$$\Delta\lambda_{\text{filter 005}} = 4.35\,\text{nm} \mathrel{\widehat{=}} 2.14\,\text{THz}. \tag{3.11}$$

These tuning ranges have been measured by turning the filter as far as the kinematic mounts allow, which can be seen in Figure 3.19. The tuning range is then calculated by subtracting the smallest and the largest wavelength that have been measured from one another. The occasional mode hops that appear in the plots, especially those that are visible in the curve for IFL005, have not been included in this because they do not correspond to the filter angles and are instead caused by the turning of the screws which cannot be done in a very smooth way due to spatial limitations.

The tuning ranges are not smooth but have smaller mode hops of around 20 GHz after only a couple of screw turns, which means the fine-tuning of the wavelength might have to be done by current and temperature adjustments along with changing the filter angle.

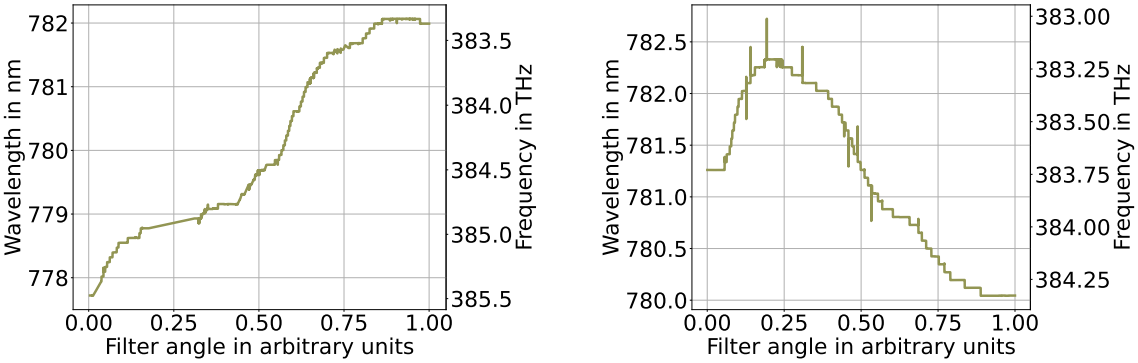

(a) Tuning range of IFL004 at 17.3 °C

(b) Tuning range of IFL005 at 24 °C

Figure 3.19: Tuning ranges achieved by changing the interference filters' angle in both lasers. The angle is varied in between −6° and 12° with respect to the output beam. The variation is not uniform due to spatial limitations when turning the screws. For this reason the x-axis is given in arbitrary units instead of filter angle.

CHAPTER 4

Characterization of the Interference Filter Lasers

In this chapter the refurbished lasers' characteristics are being described. At first the power and wavelength of the laser as function of diode current are characterized in Equation 4.1. The stability and the beamprofile are presented in section 4.3 and section 4.2.

4.1 Current-Power-Frequency-Characterization

The output power largely depends on the diode current. The basic principle explaining this is the following: The current is sent though a p-n semiconductor diode in forward direction, allowing for electron-hole recombination in the p-n junction. The recombination energy is emitted as photons with the wavelength depending on the band gap energy. The emitted photons are reflected from the ends of the diode causing induced emission in the p-n junction. Once a threshold current is reached, the induced emission rate is greater than the spontaneous emissions [9, pp.316-317]. Above this threshold the increasing number of electrons passing through the diode causes a linear increase in the number of emitted photons and therefore the output power. This can be described as

$$P_{\text{out}} = \eta_P (I - I_{\text{thr}}) \tag{4.1}$$

with P_{out} being the output power, η_P being the slope coefficient and I_{thr} being the threshold current. With η_P one can also calculate the quantum efficiency which describes the rate of emitted photons per electron going into the diode. This is calculated in subsection 4.1.1.

Besides the power the output wavelength also depends on the diode current. As mentioned previously, the emitted wavelength depends on the energy of the band gap in the diode. While this largely depends on the semiconductor that makes up the diode, it also changes with temperature. A temperature change also causes a change in the refractive index and the cavity length of the diode. Both of these effects cause the emitted wavelength to grow larger for increasing temperatures [11]. Raising the diode current has the same effect, causing a linear relation between the diode current and the emitted wavelength that is examined in subsection 4.1.2.

4.1.1 Current-Power

As previously explained the current dependency of the output power is an important characteristic of a laser. To examine it the plots in Figure 4.1 are measured.

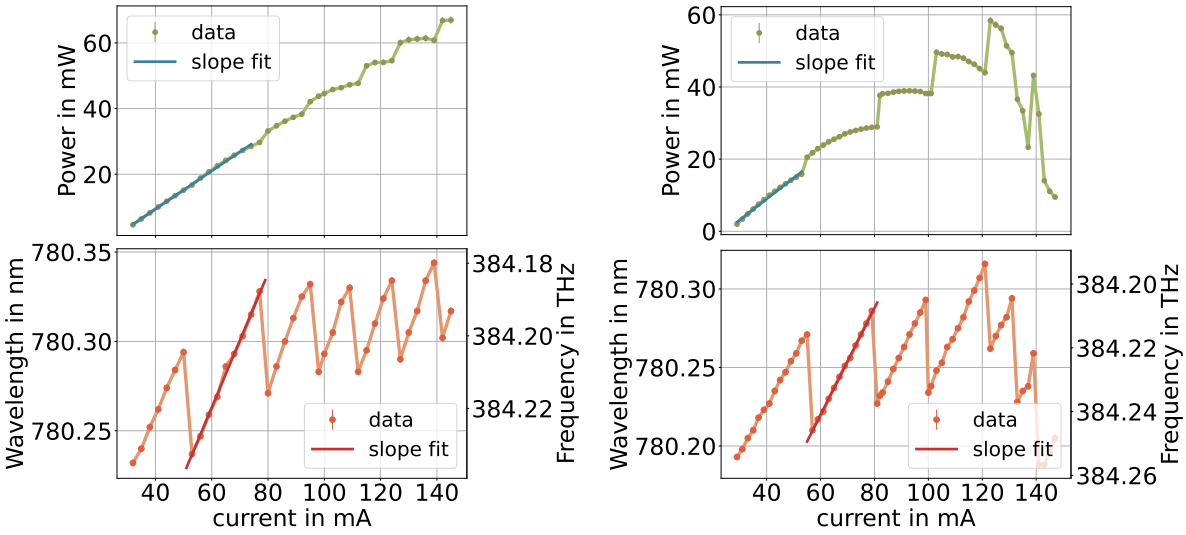

(a) Measurement for IFL004

(b) Measurement for IFL005

Figure 4.1: Current-Power-Frequency characterization plots for both refurbished lasers. The errorbars in all four plots are too small to be visible.

While the plots look as expected for lower diode current, e.g. grow approximately linearly, this isn't true for the entire curve, especially for IFL005. Besides rather large mode hops which also cause power jumps[1] with increasing currents the output power also decreases with increasing currents between these jumps and at them. This effect grows with increasing power, until at 122 mA and higher currents it is so extreme that the output power rapidly drops with increasing current. It can be explained by looking at the diode's output for larger injection currents: as the current increases not only does the emitted wavelength grow larger, the output also gets more and more multi-mode which could be seen on the wavemeter. Since larger wavelengths are not transmitted (or not as well) by the interference filter, the output power decreases. The multi-mode output barely affects the laser's output power for lower diode currents, but for higher diode currents the described power decrease in between mode hops becomes obvious [12].

By fitting a linear function to the current-power curve in the interval before the first mode hop a power slope can be determined. For IFL004 this interval is in between 27 mA and 77 mA, for IFL005 it is much smaller and only goes from 27 mA to 53 mA. The power slopes are

$$\left(\frac{\Delta P}{\Delta I}\right)_{004} = (0.5737 \pm 0.0061)\,\mathrm{W/A} \tag{4.2}$$

$$\left(\frac{\Delta P}{\Delta I}\right)_{005} = (0.595 \pm 0.015)\,\mathrm{W/A}\,. \tag{4.3}$$

[1] This can be seen very well when comparing the upper and lower plot in Figure 4.1

With these slopes the quantum efficiency η of the two can be calculated. It describes the number of photons emitted per number of electrons sent into the diode. By comparing the slope of an ideal laser [13]

$$\left(\frac{\Delta P}{\Delta I}\right)_{\text{ideal}} = \left(\frac{\Delta E/t}{\Delta Q/t}\right)_{\text{ideal}} = \frac{\mathrm{h}\frac{\mathrm{c}}{\lambda}}{q_{\mathrm{e}}} \tag{4.4}$$

to that of the two IFLs, the quantum efficiency is calculated. Here $\Delta E/t$ is the emitted energy per time (in J/s), $\Delta Q/t$ the charge transferred into the diode per time (in C/s), h the Planck constant and q_{e} the electron charge. The quantum efficiencies for the two lasers are

$$\eta_{004} = (37.39 \pm 0.95) \times 10^{-2} \tag{4.5}$$

$$\eta_{005} = (36.05 \pm 0.39) \times 10^{-2}. \tag{4.6}$$

Comparing this to the quantum efficiencies of the commercial ECDLs used in the RQO experiment, one can see that the quantum efficiencies of both types of lasers are approximately the same[2].

To get an idea for the maximum possible output power, the power for both lasers at a diode current of 100 mA is measured. For both lasers there are two mode hops in the measurement before getting to 100 mA, when thinking about the maximum output power it is important to keep in mind that the mode hops become more frequent with increasing currents until the output power becomes unstable.

$$P_{100\text{mA }004} = (44.57 \pm 0.03)\,\text{mW} \tag{4.7}$$

$$P_{100\text{mA }005} = (38.19 \pm 0.03)\,\text{mW}. \tag{4.8}$$

Both lasers have a maximum operating current of 165 mA which is the maximum current for the laser diode as stated by Thorlabs.

4.1.2 Current-Frequency

After having already looked at the mode hops that occur with increasing diode currents in subsection 4.1.1, the frequency tuning using the diode current is another characterization aspect to be looked at. For this, analogously to the power scaling, a linear function is fitted to one interval between mode hops to determine the tuning slope as shown in Figure 4.1. The tuning range can be determined by looking at the largest and smallest wavelength of each of these intervals. The same approach was used in subsection 3.1.2 to determine the tuning range when tuning by temperature changes. In that case the tuning range was calculated by averaging over the single tuning ranges. This is not done here because the tuning ranges get smaller for higher currents due to the multi-mode behaviour. Instead, the biggest tuning ranges that are measured are considered as the maximum tuning range. With the wavelength

[2] The Toptica DL pro lasers in the RQO experiment have quantum efficiencies between $\eta = 21.4 \times 10^{-2}$ and $\eta = 37.1 \times 10^{-2}$

measurements in Figure 4.1 there is a slope of

$$\left(\frac{\Delta\lambda}{\Delta I}\right)_{\text{current, 004}} = (3.75 \pm 0.11)\ \text{nm/A} \mathrel{\widehat{=}} (1.848 \pm 0.050)\ \text{GHz/mA} \tag{4.9}$$

$$\left(\frac{\Delta\lambda}{\Delta I}\right)_{\text{current, 005}} = (3.400 \pm 0.032)\ \text{nm/A} \mathrel{\widehat{=}} (1.675 \pm 0.016)\ \text{GHz/mA} \tag{4.10}$$

and a maximum tuning range of

$$\Delta\lambda_{004} = (0.091 \pm 0.020)\ \text{nm} \mathrel{\widehat{=}} (45 \pm 15)\ \text{GHz} \tag{4.11}$$

$$\Delta\lambda_{005} = (0.082 \pm 0.010)\ \text{nm} \mathrel{\widehat{=}} (40.4 \pm 5.0)\ \text{GHz}. \tag{4.12}$$

Both of these results show that by adjusting the diode current, the wavelength can be finetuned quite well. However, as for using the temperature for finetuning, finetuning with the current gets less efficient for higher currents. It is possible to reduce the number of mode hops and the power drops caused by this by lowering the laser temperature. It is however not possible to remove the mode hops and the power drops completely, as this would require going to temperatures so low that side effects such as water condensation inside of the housing would occur. This would not be sustainable for running the laser as they are.

4.2 Beamprofile

A Gaussian beam profile is desirable for many applications in an optics lab. It allows efficient mode matching, for example for fiber coupling or cavity coupling. To get a picture of the beamshape a camera[3] is put in the output beam of the laser. In order not to saturate (and possibly damage) the sensor, a filter with ND= 7.0[4] is added in between the laser and the camera. The images taken with the camera can be seen in Figure 4.2. With these photos, Gaussian curves are fitted to the beamprofile to obtain the beamwaists:

$$\begin{aligned}&\text{IFL004 :}\\ &\omega_{0,x} = (0.9734 \pm 0.0063)\ \text{mm} \qquad \omega_{0,y} = (1.3067 \pm 0.0047)\ \text{mm}\end{aligned} \tag{4.13}$$

$$\begin{aligned}&\text{IFL005 :}\\ &\omega_{0,x} = (1.2261 \pm 0.0069)\ \text{mm} \qquad \omega_{0,y} = (2.154 \pm 0.012)\ \text{mm}.\end{aligned} \tag{4.14}$$

It is important to note that the beam waist is not defined as the half width half maximum, but instead as the value where the intensity has dropped to $1/e^2$ [14, p.79].
Both laser beams are relatively small in diameter, but not very round. Especially the profile of IFL005's beam has an ellipticity with a long horizontal and a short vertical axis. This can cause some problems in the beam characterization, one example for this being working with a shear plate interferometer (as described in subsubsection 3.1.2) where the shear plate has to be chosen by diameter which assumes a round profile.

[3] Arducam Model MT9J001 (12-bit)
[4] ND stands for neutral density.

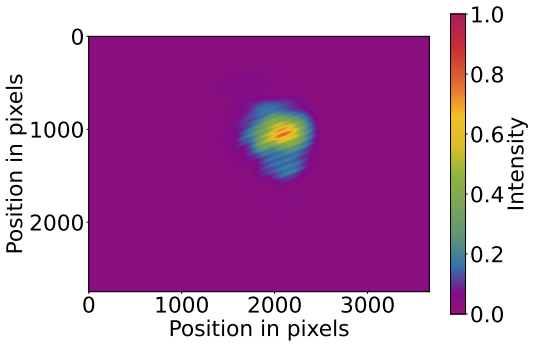

(a) Profile for IFL004

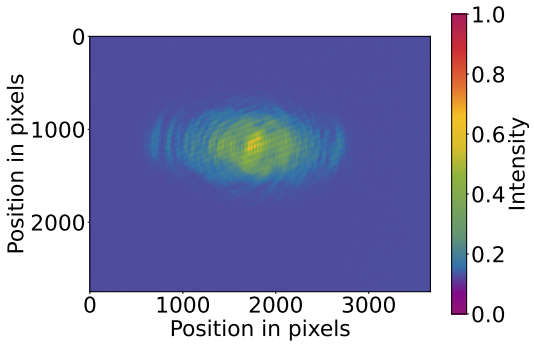

(b) Profile for IFL005

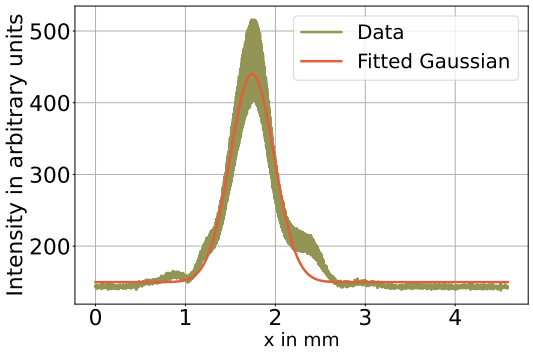

(c) Horizontal beamprofile for IFL004

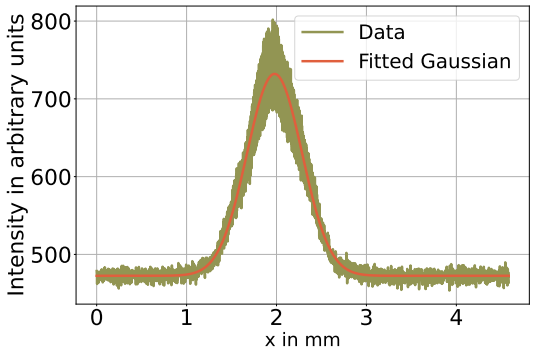

(d) Horizontal beamprofile for IFL005

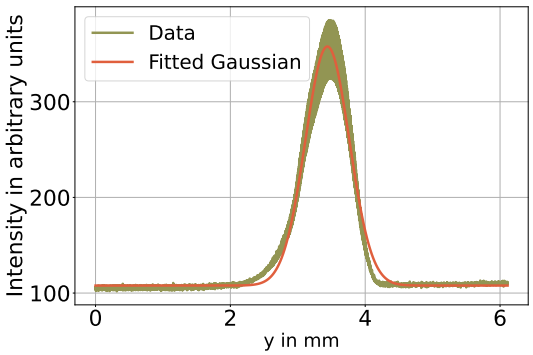

(e) Vertical beamprofile for IFL004

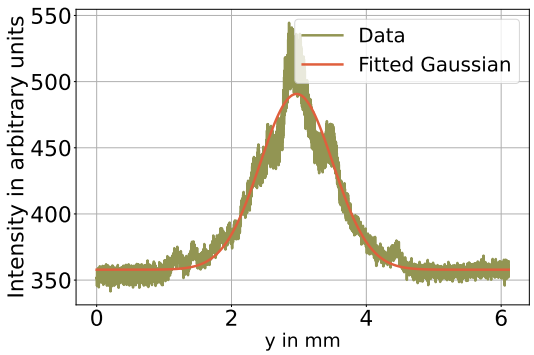

(f) Vertical beamprofile for IFL005

Figure 4.2: Images of the laser beams taken at a distance of 7 cm and a diode current of 32 mA.

4.3 Stability

Frequency stable lasers are an important tool for performing cold atom experiments. The frequency stability of a free running laser is an important characteristic to determine external noise sources that cause frequency drifts on the minute to hour timescale. This characteristic is examined in two parts: the short-term frequency fluctuations and the wavelength drift over longer time spans. For the short-term measurement, the two beams are not analyzed independently, but instead a beatnote signal is used. The beatnote is used because it gives insights into kHz changes, whereas the wavemeter can measure stability on a completely different scale. For this the two beams are overlapped on a photodiode and the beatnote is monitored on a signal analyzer. The latter is checked by recording the wavelength overnight using a wavemeter.

4.3.1 Beatnote of the free running Lasers

To examine the short-term frequency stability of both lasers, the beatnote of the two is measured. The beatnote is an interference signal created by the sum of the electric field of the two beams. The best interference signal can be achieved when the two electric field overlap exactly. Thus, the polarizations of both lasers are equalized, their wavelengths are brought close to one another and the beams are overlapped on a photodiode. The setup for this is shown in Figure 4.3.

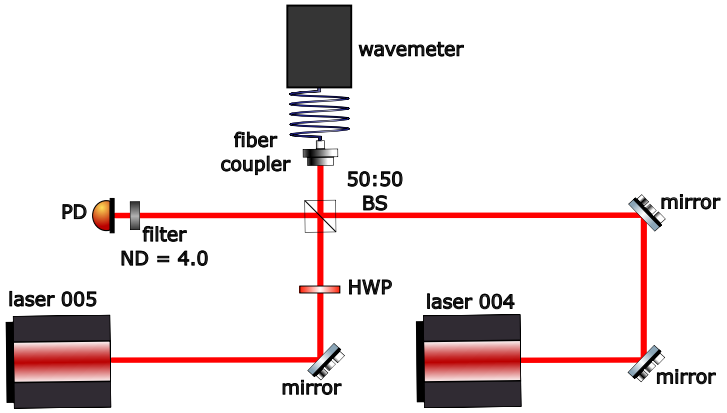

Figure 4.3: Setup for monitoring the beat signal of the two lasers. IFL005 is sent through a half-wave plate (HWP) to equalize the polarizations of both beams. The beams are overlapped on a 50:50 beamsplitter. This overlap is monitored on photodiode (PD). The wavelength of both beams can be checked with the wavemeter.

A single beatnote resonance peak is measured to get a rough estimate of the combined linewidth (shown in Figure 4.4(a)). After this, a trace is recorded for two minutes using the *maximum hold* function on the signal analyzer. This measurement shows the maximum intensity recorded for each frequency during the measuring time. The peak's width shows the fluctuation of the frequency difference for the two lasers (Figure 4.4(b)).

The resonance peak, which is at the beat frequency $\nu_{\text{beat}} = |\nu_1 - \nu_2|$, has a linewidth of [15]

$$\Delta\nu_{\text{beat}} = \sqrt{\Delta\nu_{L1}^2 + \Delta\nu_{L2}^2}\,. \tag{4.15}$$

Here the combined linewidth is estimated to be around 400 kHz. This is estimated from the capture and

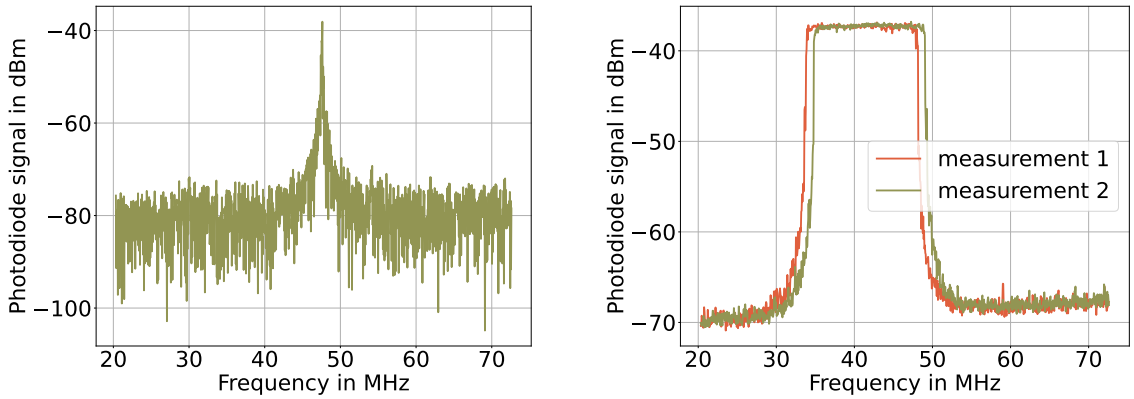

(a) Single resonance peak measurement on the spectrum analyzer with sweep time 9.4 ms and resolution bandwidth 82 kHz.

(b) Resonance shifts recorded over two minutes with the maximum hold function on the spectrum analyzer.

Figure 4.4: Beatnote measurement for the two IFLs

is only meant to give an order of magnitude, not to give a precise measurement. The estimate is based on a single capture from the signal analyzer, and can therefore not be assumed to correctly give the actual combined linewidth.

The two-minute recordings show fluctuation widths of

$$\Delta\nu_{2\text{min},\,1} = (14.59 \pm 0.43)\,\text{MHz} \tag{4.16}$$

$$\Delta\nu_{2\text{min},\,2} = (14.94 \pm 0.36)\,\text{MHz} \tag{4.17}$$

$$\Rightarrow \Delta\nu_{2\text{min},\,\text{avg}} = (14.80 \pm 0.28)\,\text{MHz}. \tag{4.18}$$

This makes sense - both lasers are running free and are somewhat stable, so their difference can fluctuate a bit as well.

4.3.2 Long-term Wavelength Stability

Using the same setup as for the beatnote measurement shown in Figure 4.3, the wavelength fluctuations over longer time scales are measured. For this the wavelength is recorded over approximately 14 h using the wavemeter. Both lasers drift (450 ± 50) MHz during this time, which shows that they are running relatively stable. When comparing the data from this measurement to that of the 2 min-hold beatnote one can see that in both cases the frequency fluctuates by roughly 15 MHz over the course of 2 min. This long-term measurement also shows that the wavelength does not just fluctuate but also actually shifts over longer periods of time, which was not visible in the short-term beatnote measurement.

With these stability measurements, the foundation for frequency locking the lasers to one another using the beatnote signal is created. It was not done within the scope of this thesis, but is a future goal for the two lasers.

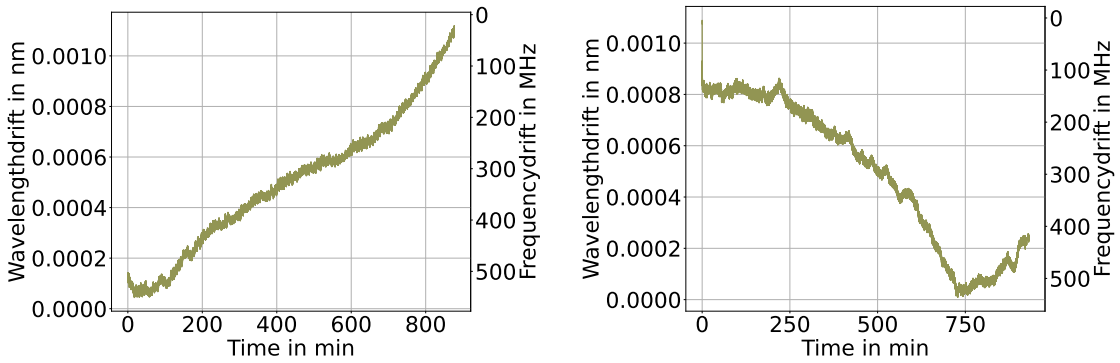

(a) Measurement for IFL004, the origin for the drift is approximately 780.2435 nm.

(b) Measurement for IFL005, the origin for the drift is approximately 780.2428 nm.

Figure 4.5: Overnight-Wavelength shift for both refurbished lasers

4.4 Tuning the Wavelength

From the design of the laser one can conclude which parts of the laser one can apply feedback to.

To compensate for fast fluctuations and to tune the wavelength, it is easiest to use the diode current as discussed in subsection 4.1.2. While the temperature can also be used to adjust the wavelength, it does not make sense to use it for feedback as it is very slow. For slow fluctuations it makes more sense to use the piezo actuator for compensation. Changing the lasers' wavelength using the piezo is the subject of the next chapter, where the wavelength is scanned for a first application of the lasers.

CHAPTER 5

Absorption Spectroscopy of Rubidium

The two refurbished lasers are used for Rubidium spectroscopy, after having been characterized in detail. To understand the Rubidium spectroscopy signal, it is important to understand the level scheme. There are different methods to optically investigate the energy levels of an atom. In Doppler broadened absorption spectroscopy the laser drives atomic transitions which allows for the energy levels to be resolved. This method is restricted in resolution due to atomic movement causing broadened linewidths. Doppler free absorption spectroscopy removes this effect, which makes it possible to resolve smaller structures in the spectrum. This is explained in more detail in subsection 5.2.1.

Absorption spectroscopy can be done with a relatively simple setup, which is described in section 5.1. For a more detailed look at the spectrum, the setup is then expanded to do saturated or Doppler-free spectroscopy where the hyperfine splitting between energy levels can be resolved. This is described in section 5.2. The laser is scanned using the piezo which has a limited range. To increase the scan range, a current feedforward mechanism is then implemented and analysed in section 5.3.

5.1 Absorption Spectroscopy (Doppler broadened)

5.1.1 Theory

When working with Rubidium, there are two isotopes that are stable and therefore relevant to the level scheme. Natural Rubidium is made up of (72.17±0.02) % ^{85}Rb and (27.83±0.02) % of ^{87}Rb [16, p.760]. Technically, only ^{85}Rb is stable, since ^{87}Rb is β^--active. However, it has a half life of $(4.88\pm5.00)\times10^{10}$ years and can thus be considered stable for the purposes of this work [16, p.760]. For both of these isotopes the atomic transition frequencies between the levels $5S_{1/2}$ and $5P_{3/2}$ are approximately 384 THz, which corresponds to a wavelength around 780 nm. This is why the lasers used for this thesis were chosen to have a wavelength of 780 nm.

Since Rubidium is an alkali, meaning it has a single outer electron, the fine and hyperfine structure of the level scheme and therefore the nuclear spin of both ^{85}Rb and ^{87}Rb has to be considered. The nuclear spin of ^{85}Rb is $I = 5/2$ and that of ^{87}Rb is $I = 3/2$ [17]. With $\vec{F} = \vec{J} + \vec{I}$ we get $F = 2, 3$ for the ^{85}Rb $5S_{1/2}$ state and $F = 1, 2$ for the ^{87}Rb $5S_{1/2}$ state. With the selection rule for electric dipole transitions $\Delta J = 0, \pm1 (0 \nleftrightarrow 0)$ [18, p.224] and a fixed nuclear spin I, the transitions regarded here follow $\Delta F = 0, \pm1$. The transitions that are possible with these specifics are shown in Figure 5.1.

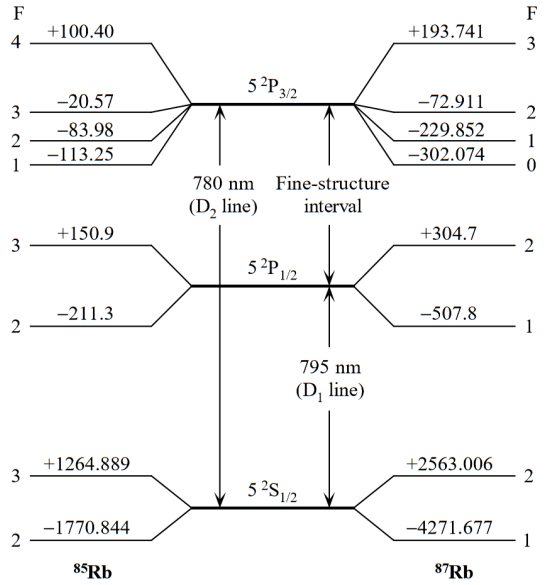

Figure 5.1: Level scheme for $5S_{1/2}$ and $5P_{3/2}$ levels of ^{85}Rb and ^{87}Rb (taken from [19]). The hyperfine splitting is in units of MHz in regard to the unperturbed states. The $5P_{1/2}$ level and D1 line are not considered here.

Isotope	F → F'	Frequency offset
^{87}Rb	1 → 2	5 501.7 MHz
	(1 → 1)(1 → 2)	5 423.2 MHz
	(1 → 0)(1 → 2)	5 387.1 MHz
	1 → 1	5 344.7 MHz
	(1 → 0)(1 → 1)	5 308.6 MHz
	1 → 0	5 272.75 MHz
^{85}Rb	2 → 3	2 975.3 MHz
	(2 → 2)(2 → 3)	2 943.5 MHz
	(2 → 1)(2 → 3)	2 928.9 MHz
	2 → 2	2 911.8 MHz
	(2 → 1)(2 → 2)	2 897.2 MHz
	2 → 1	2 882.6 MHz
	3 → 4	60.5 MHz
	(3 → 3)(3 → 4)	0 MHz
	(3 → 2)(3 → 4)	−31.7 MHz
	3 → 3	−60.5 MHz
	(3 → 2)(3 → 3)	−92.2 MHz
	3 → 2	−123.9 MHz
^{87}Rb	2 → 3	−1 066.4 MHz
	(2 → 2)(2 → 3)	−1 199.7 MHz
	(2 → 1)(2 → 3)	−1 278.2 MHz
	2 → 2	−1 333.0 MHz
	(2 → 1)(2 → 2)	−1 411.5 MHz
	2 → 1	−1 489.9 MHz

Table 5.1: Possible transitions in Rb85 and Rb87 ($5S_{1/2} \rightarrow 5P_{3/2}$) considering hyperfine splitting of ground and excited state. Frequency offset relative to ^{85}Rb F = 3 → F'

The energy levels can be visualized using absorption spectroscopy: a laser passes through an atomic cloud and if it is on resonance with a transition of the atoms, the laser light will be scattered or absorbed and reemitted in an arbitrary direction. Therefore, by scanning the laser wavelength, it is possible to map out the cloud's transitions by observing the intensity of the laser as a function of wavelength.

By scanning through a certain interval of wavelengths with the laser, different transitions are driven by it. When monitoring the transmission signal for this laser one gets an *atomic spectrum*. The atoms in the medium have a thermal distribution of velocity, the Maxwell-Boltzmann-distribution, which means that for every temperature higher than 0 K atoms have a certain velocity. Due to the Doppler-shift, the observed frequency ν_{obs} for the atoms depends on their velocity parallel to the propagation direction v of the laser beam with [18, p.229]

$$\nu_{\text{obs}} = \nu_0 \cdot \left(1 - \frac{\text{v}}{\text{c}}\right). \tag{5.1}$$

Here ν_0 is the laser's frequency and c the speed of light.

The intensity I of absorbed laser light as a function of frequency can be described as [18, p.230]

$$I(\nu_{\text{obs}}) \propto \exp\left(-\frac{m_{\text{atom}}c^2}{2\text{k}_B T} \cdot \left(\frac{\nu_0 - \nu_{\text{obs}}}{\nu_0}\right)^2\right), \tag{5.2}$$

where m_{atom} is the mass of the atom, k_B the Boltzmann constant and T the temperature in K. This intensity distribution, the so-called Doppler profile, has a linewidth ν_{FWHM} of [18, p.230]

$$\nu_{\text{FWHM}} = \frac{2\nu_0}{c}\sqrt{2\ln(2)\frac{k_B T}{m_{\text{atom}}}}\,. \tag{5.3}$$

This broadening compared to the natural linewidth is referred to as Doppler broadening. Because of it, the resolution of the atomic spectra is highly dependent on the temperature of the medium, which is why this method is also referred to as Doppler-broadened absorption spectroscopy. In the given setup the linewidth for $5S_{3/2}$ compared to the Doppler broadened linewidth is [20]

$$\nu_{\text{natural}} = (6.062 \pm 0.017)\,\text{MHz} \tag{5.4}$$

$$\nu_{\text{Doppler}} = (515.591 \pm 0.014)\,\text{MHz}. \tag{5.5}$$

The Doppler broadened linewidth was calculated assuming a room temperature of (300±2) K, a Rubidium mass of (85.4678±0.0003) u [16] and a frequency ν_0 of (384.230484468±0.000000010) MHz [19].

As a result of this, the spectra achieved with Doppler broadened spectroscopy in subsection 5.1.2 cannot resolve the hyperfine levels, as these usually have a scale around 100 MHz.

5.1.2 Measurements and results

In the setup shown in Figure 5.2 the beam is sent through a glass cell filled with Rubidium where it can be absorbed by the atoms. The transmission signal is then detected by a photodiode (PD2). In order to do spectroscopy a signal generator is connected to the piezo BNC-connector at the back of the laser. With this, ramp signals of up to 20 V_{pp} can be put on the ring piezo that is part of the cat eye construction. The laser can now scan through a certain interval of wavelengths that is proportional to the applied piezo voltage. Since the wavelength changes with time, the scanned absorption spectrum can be monitored on an oscilloscope.

With this setup it is possible to scan one dip in the D2 line of Rubidium as shown in Figure 5.3. Note that the spectroscopy signal (PD2) has been scaled up to make the dip structure more visible. The spectrum was captured in the *High resolution* mode of the oscilloscope, which means that the oscilloscope averages the data in each recorded bin, contrary to the normal acquisition mode where one random datapoint per bin is displayed. This effectively reduces the random noise on the signal and produces clearer spectra, which is why it is used for all the oscilloscope captures for the spectroscopy in this thesis unless stated otherwise.

Since just one dip can be seen, it is not possible to identify with certainty which dip this is. The wavemeter can be used to assist with identifying the dip, but the spectrum cannot be resolved in full detail. Using the wavemeter one can see that it is possible to scan up to approximately 2 GHz.

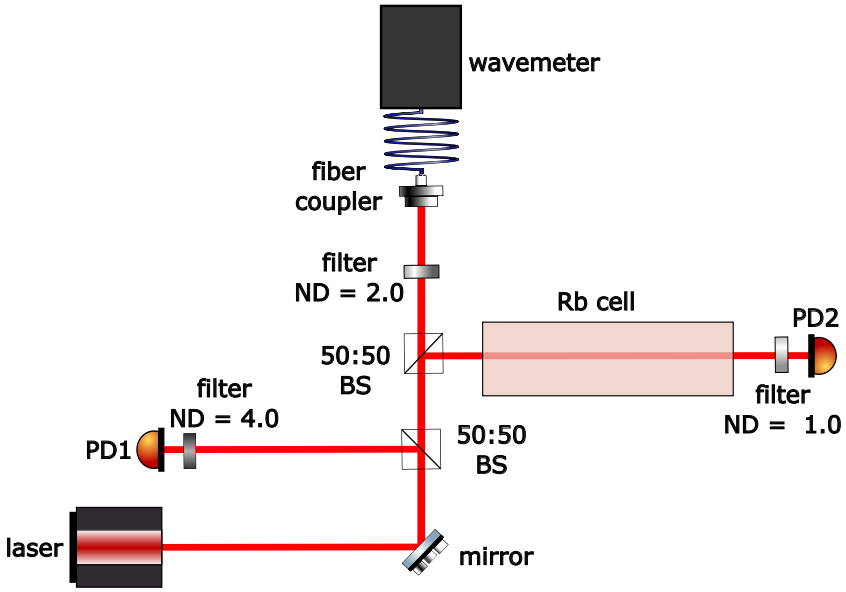

Figure 5.2: Experimental setup for measuring Doppler broadened absorption Spectroscopy. The laser's initial intensity is monitored on the first photodiode (PD1) which is covered with a neutral density (ND) filter so it does not saturate. The transmission signal behind the rubidium cell is monitored by PD2, this shows the absorption spectrum when scanning the wavelength. To have a reference for the wavelength, the beam is split up before the spectroscopy setup and part of it is coupled into a wavemeter.

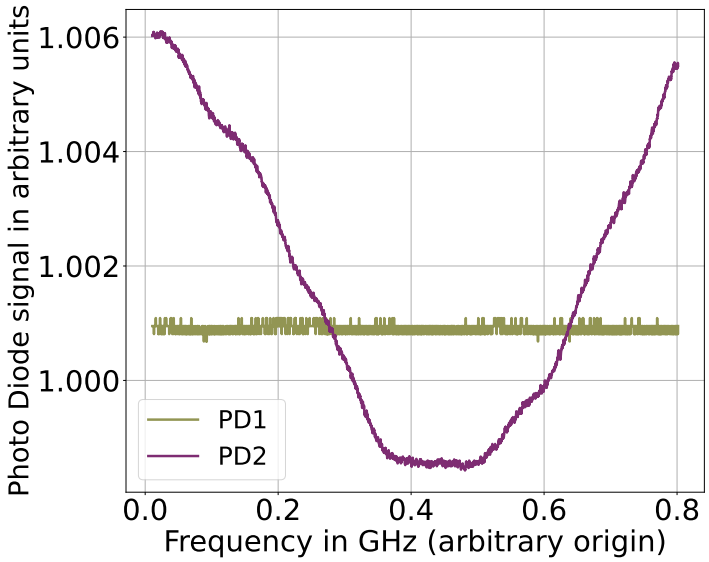

Figure 5.3: Oscilloscope capture for Rubidium absorption spectroscopy showing the ^{85}Rb F = 2 $\rightarrow$ F$'$ transition

5.2 Saturated absorption spectroscopy (Doppler-free)

Doppler broadened spectroscopy is highly limited in its resolution without drastically cooling the absorbing medium down. Since the goal is to resolve the hyperfine levels as well, a new method is needed. By using the saturation of atomic transitions, the Doppler broadening can be overcome. This is what is done in so-called *Saturated absorption spectroscopy* or *Doppler free spectroscopy*. It allows for much better resolution without cooling the absorptive medium.

5.2.1 Theory

To explain saturated absorption spectroscopy, a two level system is assumed for every atom. In contrast to Doppler broadened spectroscopy not one but two beams are used: The stronger *pump beam* excites the atoms in the medium and ideally equalizes the atomic populations in the ground and the excited state. A second, much weaker beam, the *probe beam*, is overlapped exactly with the first one. The two beams are counter-propagating and have the same wavelength.

To understand the effect of saturated absorption spectroscopy, it is easiest to first look at a beam wavelength that is slightly detuned from the atomic transition. Due to the Doppler-shift that comes with the thermal velocity[1] of the atoms, there will be some atoms that get excited by this detuned laser beam. Since the pump and probe beam are counter-propagating, they excite atoms with velocities opposite in sign as long as their frequency is detuned from resonance. In the spectrum of the probe beam this looks like regular absorption spectroscopy. However, when the lasers are exactly on resonance they both interact with the same atoms, those that have no velocity along the lasers' propagation axis. With the pump beam having excited most of these atoms to the excited state, there's a significant decrease in the absorption of the probe beam [21]. The absorption dips at the resonance wavelength that are caused by this are called *Lamb dips* and can be seen as transmission peaks within the absorption lines in the atomic spectrum [22].

5.2.2 Measurements and Results

In order to go from Doppler broadened to Doppler free absorption spectroscopy, the setup is extended as shown in Figure 5.4. Previously, the laser beam was detected by a photodiode right behind the Rubidium cell. In this extended setup it is reflected back into the cell by adding a mirror. A filter is used to regulate the probe beam's intensity and a quarter wave plate controls its polarization[2]. The mirror is mounted on a kinematic mount, so that its angle can be adjusted to precisely overlap the pump and probe beam. The probe beam is then detected by a photodiode (PD2) which connects to an oscilloscope. Also monitored on the oscilloscope are the pump beam intensity (signal of PD1) to compare the intensity of the two beams, and the piezo signal for a better view of the scan range. One spectrum that has been captured with the oscilloscope can be seen in Figure 5.5.

By adjusting both the laser current and the piezo signal, all four absorption dips can be scanned through, an overview of which can be seen in Figure 5.6. To get a result as clear as this one, some

[1] The component of the thermal velocity that is parallel to the laser's direction of propagation

[2] With the beam going through the quarter wave plate twice and being reflected on the mirror its polarization is rotated by 90°, which is needed so it is transmitted by the PBS.

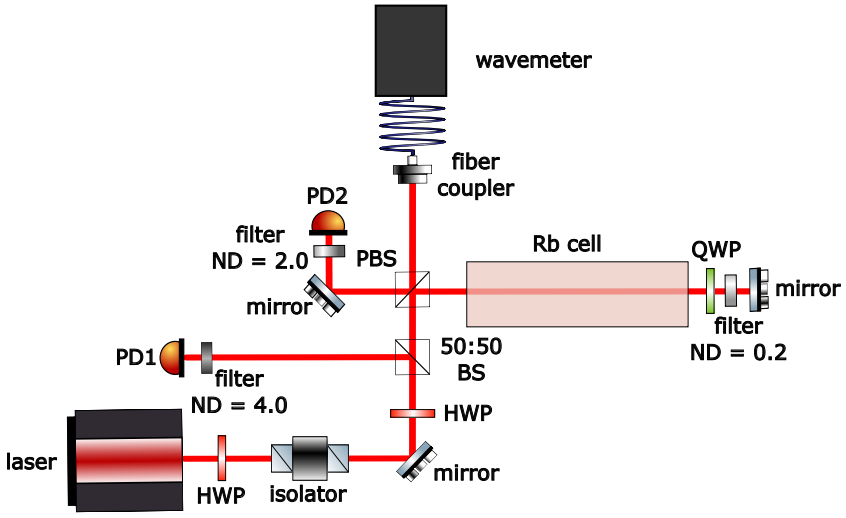

Figure 5.4: Experimental setup for measuring Doppler free Absorption Spectroscopy. The pump beam intensity is monitored on the first photodiode (PD1) which is covered with a neutral density (ND) filter so it does not saturate. The pump beam goes through the rubidium cell and is mirrored back (with a polarization orthogonal to the pump beam due to the quarter-wave plate (QWP) to create a probe beam for Doppler free Spectroscopy. PD2 detects the absorption spectrum when the wavelength is scanned. To have a reference for the wavelength, the beam is split up before the spectroscopy setup and part of it is coupled into a wavemeter.

adjustments are made: A fraction of the laser light is always sent onto the wavemeter to coarsely monitor the laser wavelength. The amount of light going to the wavemeter versus the spectroscopy can be controlled with the half-wave plate that is followed by a PBS. The power sent into the spectroscopy setup needs to be limited in order to avoid power broadening. This becomes much more relevant for the probe beam power, which can be individually controlled by adding an ND filter behind the Rubidium cell. Since the beam passes through the filter twice, a filter with a low optical density is sufficient. After trying out different options, a filter with ND = 0.2 shows the best contrast for the lamb dips, creating a pump to probe power ratio of $1 : 0.43$ and is included in the setup.
Another adjustment that is made to improve the line contrast is to optimize the overlap of pump and probe beam inside of the vapor cell. This is repeated until the size of the lamb dips is as high as possible.

One goal with this spectroscopy is to scan through as much of the D2 line as possible. The mode hop free tuning range is limited when only using the piezo for frequency tuning. The different gain and resonance spectra of laser diode, IF and external cavity need to be best overlapped. The mode hop free tuning range by only varying the external cavity length is limited. The maximum scan range in this configuration depends on the part of the spectrum that is being scanned and ranges from 1.6 GHz to 2.4 GHz for both lasers. A spectrum where around 1.6 GHz are scanned is shown in Figure 5.7. The scan range can be extended by additionally, with a given proportionality factor, modulating the laser diode current.

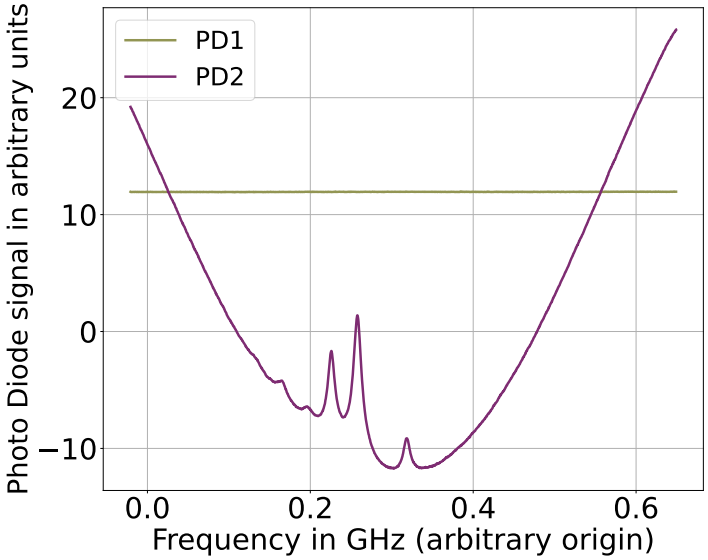

Figure 5.5: Doppler free absorption spectroscopy of the ^{85}Rb F = 3 $\longrightarrow$ F$'$ transition

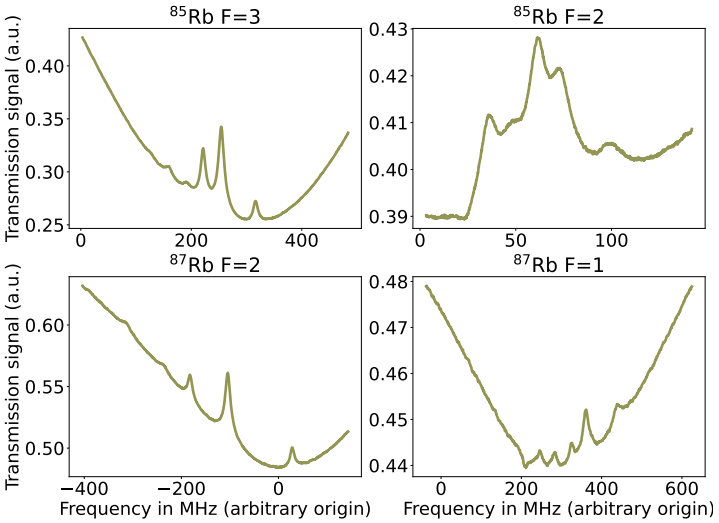

Figure 5.6: Individual dips for Doppler free absorption spectroscopy of the Rubidium D2 line, scanned with IFL004. The lamb dips are not centered within the Doppler valley due to the scan being too fast.

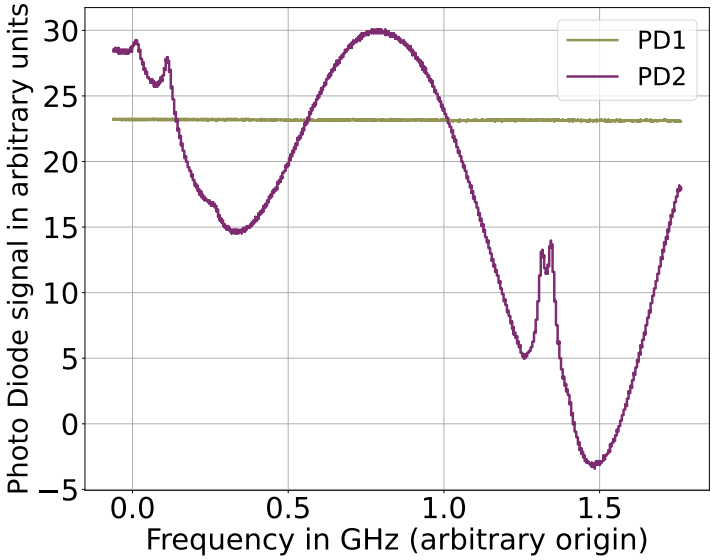

Figure 5.7: Maximum scan range Doppler free spectrum showing the ^{87}Rb F = 2 → F′(left) and ^{85}Rb F = 3 → F′(right) transitions

5.3 Increasing the Scan Range with Current Feedforward

In order to increase the scan range beyond the 2.4 GHz that can be reached by simply adjusting the piezo voltage, a current feedforward mechanism can be implemented: Along with the ramp signal for the piezo a second ramp signal is used to modulate the laser's current. This second signal is in phase with the piezo signal. Its amplitude is proportional to that of the piezo signal as well. With this method the diode's emitted wavelength is tuned along with the increasing length of the cavity which significantly increases the mode hop free tuning range.

By analysing the effectiveness of this method for different current modulation amplitudes, the scan range can be maximized. To do this quantitatively, the so-called feedforward factor (FFF) and how the mode hop free tuning range changes with it is inspected. The FFF characterizes the ratio of the current modulation and the piezo signal's amplitudes. It can be calculated as

$$\mathrm{FFF} = \frac{A_{\mathrm{CM}}}{A_{\mathrm{P}}} \cdot \mathrm{CM} \tag{5.6}$$

where A_{CM} is the current modulation signal in $\mathrm{V_{pp}}$, A_{P} the piezo voltage (also in $\mathrm{V_{pp}}$) and CM the conversion factor between the current modulation signal in V and the actual current modulation in A, a factor that is specific to the controller that is used.

The current modulation conversion factor CM for the control units is $\mathrm{CM} = 13\,\mathrm{mA/V}$. With this factor, the correlation between scan range and feed forward factor that is shown in Figure 5.8 is calculated.

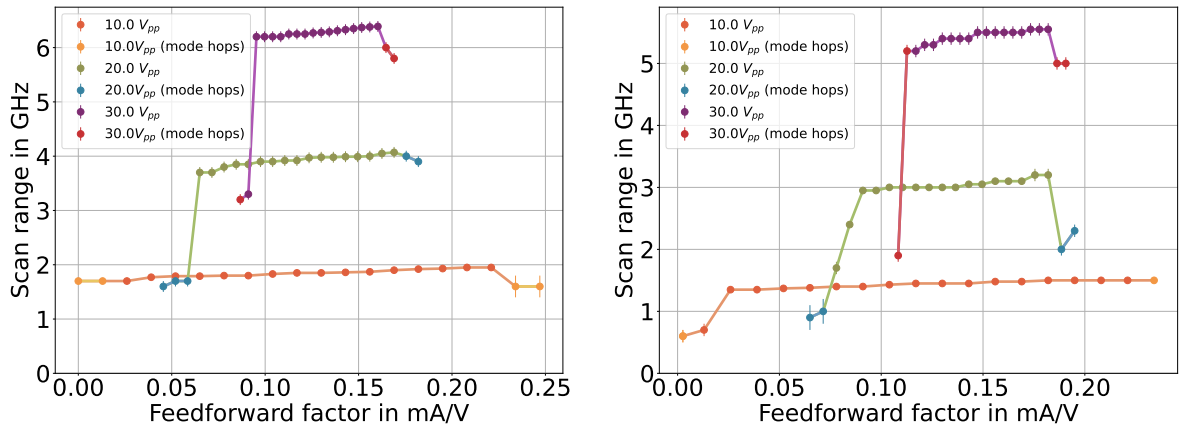

(a) Feedforward effectiveness for IFL004

(b) Feedforward effectiveness for IFL005

Figure 5.8: Scan ranges as function of feedforward factor. This is measured by varying the piezo voltage and the current modulation and recording the scan range for each of these combinations using a wavemeter.

Looking at the graph for $10\,\mathrm{V_{pp}}$ one can see that the mode hop free scan range is almost independent from the FFF. Only for very large and very small FFF the laser starts to run multimode, resulting in a drop of the scan range.

After this, the scan range is increased by choosing higher piezo voltages. Different FFFs are applied for this. For these larger scan ranges the dependency on the FFF grows. One can see that only closer to

the best FFF the piezo scan is actually compensated perfectly in phase with the current. This leads to the assumption that for even higher piezo voltages the mode hop-free range might get as small as a single optimal feed forward factor. According to the piezo manufacturer it is possible to go up to voltages of −30 V and 150 V, but for this thesis I stayed within piezo voltage ranges of ±15 V.

With the feedforward mechanism and a piezo voltage of 30 V_{pp} the maximum scan ranges are

$$\Delta\nu_{\text{scan, 004}} = 6.25\,\text{GHz} \tag{5.7}$$
$$\Delta\nu_{\text{scan, 005}} = 5.6\,\text{GHz}\,. \tag{5.8}$$

These ranges depend on which part of the spectrum is being scanned, just like in section 5.2. At the part of the spectrum where these ranges could be reached, three of the four dips in the D2 Rubidium line could be scanned. This spectrum, scanned with IFL005, can be seen in Figure 5.9. The figure also shows a corrected spectrum where the transmission signal was divided by that of the monitor photodiode to eliminate the offset in detected power that is caused by the power increase due to the current modulation.

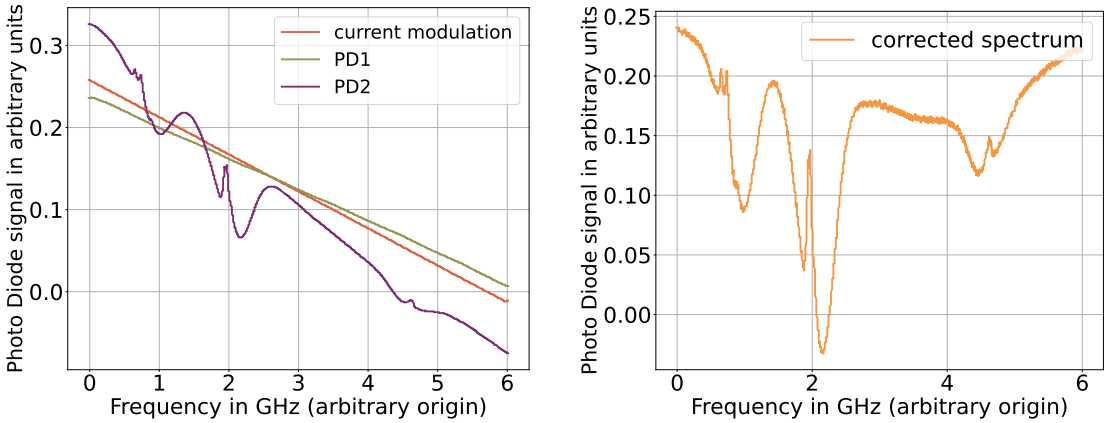

(a) Oscilloscope capture

(b) Corrected spectrum derived from a)

Figure 5.9: Maximum scan range Doppler free spectrum with feedforward mechanism for IFL005 showing the ^{87}Rb F = 2 → F′, ^{85}Rb F = 3 → F′ and ^{85}Rb F = 2 → F′ transitions

With these results, it is clear that the feedforward worked very well. It was possible to increase the scan range by a factor higher than 2 compared to the scan that only varied the cavity length. This allows the home built IFLs to be scanned over a large frequency range, comparable to that of a commercially made laser.

CHAPTER 6

Conclusion and Outlook

For this thesis I refurbished and characterized two home built interference filter lasers. They previously operated at 852 nm and were changed to 780 nm to be used in the Rubidium Rydberg quantum optics experiment. The goal of this work to have two new fully characterized lasers was reached.

In the process of refurbishing, all wavelength dependent elements were exchanged. To exchange the diodes a new way of mounting them inside the existing housing had to be developed since the housings were originally designed for diodes with a larger packaging. Along with this the interference filters used for tuning the lasers' wavelength had to be exchanged to match the new diodes' wavelength. The cavities were then closed with the existing cat eye constructions, realigning them to lower the lasing threshold as much as possible.

The refurbished lasers were then characterized in detail: The tuning ranges for the lasers achieved by varying the diodes' temperature and current, along with the tuning range of the interference filter were examined. For higher injection currents I found that both, but one of the two lasers in particular, become increasingly multi-mode which limits the output power. This effect can be reduced by lowering the diode temperature, however it cannot be completely removed since the temperature needed for this causes unwanted side effects such as water condensation inside of the housing. The maximum output power could be increased by using a different diode or an outcoupling mirror with a lower reflectivity. However, the latter would cause a broader linewidth and less stability.
Besides these relations, the beamprofile was captured with a camera, finding that only one beam had a Gaussian shape, whereas the other was more elliptical. This could limit fiber coupling efficiencies. As a final characterization aspect, the frequency stability of the two lasers was inspected. For the short term stability of both lasers, the beatnote of the two lasers was recorded, finding a fluctuation of tens of Megahertz over the timespan of several minutes. When looking at the long-term stability of both lasers, a consistent result was found. It was measured by recording the wavelength of both lasers with a wavemeter for about 14 h, during which both lasers experienced a frequency shift of around 500 MHz.

The next step in working with these lasers is stabilizing their frequency. A possible approach to do this is to frequency lock to a transition in the D2 line of the Rubidium spectrum. One could lock both lasers to this atomic reference. Alternatively, the two lasers could be stabilized with respect to each other. This is called beatnote offset lock and could be done using a delay line. Here, a phase shift depending

on the beat-frequency of the two lasers is used to create an error signal, for further information on this consider [23].

As a first application, the two lasers were used for spectroscopy of the D2 line for ^{85}Rb and ^{87}Rb. Here I set up both normal absorption spectroscopy and afterwards Doppler free spectroscopy to better resolve the hyperfine structure. Using a current feedforward mechanism, up to 6 GHz of this spectrum could be scanned by varying the cavity length. The maximum scan range is restricted by the maximum piezo voltage.

My work also aims to create a guide for building more of these interference filter lasers in the future. For this, I had a look at the established way to build them and the existing designs for the laser housings within the NQO group.

While most of the design choices were intuitive to work with, the installation of the diode in the collimation tube was rather impractical. The best solution was to glue the diode onto the retaining ring, which prevents any reuse of both the diode and the retaining ring. There is a newer version of inner laser housings that exists, which allows for a different type of collimation package. This newer package comes in different opening sizes at the front and is therefore compatible with both diode sizes that are eligible for these lasers. However, since the diode is mounted into them by screwing a retaining ring behind it just like in the current version, the diode's orientation could still be affected by stress on the connecting cables. This problem affects the diode's rotational orientation, which defines the output polarization of the laser. Due to this, making some adjustments to this part of the housing design and collimation package would greatly improve the process of setting the polarization for these lasers. Possible solutions for this could be retaining rings with a slightly increased diameter for a tighter fit within the used collimation package, or a rubber ring as part of the retaining structure that decreases unwanted movement. The latter is realized similarly in some of the aspheric lens adapters that Thorlabs offers. Other ideas for fixing this issue include mounting the diode in a thick thermal paste and fixing the cables for the diode better on the outside of the housing.

Bibliography

[1] M. Fleming and A. Mooradian,
Spectral characteristics of external-cavity controlled semiconductor lasers,
IEEE Journal of Quantum Electronics **17** (1981) 44.

[2] P. Zorabedian, "8 - Tunable External-Cavity Semiconductor Lasers", *Tunable Lasers Handbook*, ed. by F. Duarte, Optics and Photonics, San Diego: Academic Press, 1995 349.

[3] V. V. Vassiliev et al., *Vibration-proof ECDL with an Intracavity Interference Filter*,
Bulletin of the Lebedev Physics Institute **46** (2019) 309.

[4] X. Baillard et al., *Interference-filter-stabilized external-cavity diode lasers*,
Optics Communications **266** (2006) 609.

[5] W. Hong and O. J. Painter,
"Design and Characterization of a Littrow Configuration External Cavity Diode Laser", 2005.

[6] P. Zorabedian and W. R. Trutna,
Interference-filter-tuned, alignment-stabilized, semiconductor external-cavity laser,
Optics Letters **13** (1988) 826.

[7] K. C. Harvey and C. J. Myatt,
External-cavity diode laser using a grazing-incidence diffraction grating,
Optics Letters **16** (1991) 910.

[8] A. L. Lyubarsky, B. Falsini, M. E. Pennesi, P. Valentini and E. N. Pugh,
UV- and Midwave-Sensitive Cone-Driven Retinal Responses of the Mouse: A Possible Phenotype for Coexpression of Cone Photopigments, The Journal of Neuroscience **19** (1999) 442, Fig. 1.

[9] W. Demtröder, *Laser Spectroscopy*, Berlin, Heidelberg: Springer Berlin Heidelberg, 2008,
ISBN: 9783540734154 9783540734185.

[10] *Collimation tube*, LT230P-B, Rev. F, Thorlabs, 2022.

[11] G. Galbács, *A Review of Applications and Experimental Improvements Related to Diode Laser Atomic Spectroscopy*, Applied Spectroscopy Reviews **41** (2006) 259.

[12] A. Martin, P. Baus and G. Birkl, *External cavity diode laser setup with two interference filters*,
Applied Physics B **122** (2016) 298.

[13] K. S. Mobarhan, *Test and characterization of laser diodes: determination of principal parameters*,
Newport Corporation (1995).

[14] B. E. A. Saleh and M. C. Teich, *Fundamentals of photonics*, Third edition,
Wiley series in pure and applied optics, Hoboken, NJ: Wiley, 2019, ISBN: 9781119506874.

[15] S. V. Kashanian et al., *Noise spectroscopy with large clouds of cold atoms*,
Physical Review A **94** (2016) 043622.

[16] J. R. De Laeter et al., *Atomic weights of the elements. Review 2000 (IUPAC Technical Report)*, Pure and Applied Chemistry **75** (2003) 683.

[17] S. Millman and M. Fox, *Nuclear Spins and Magnetic Moments of Rb 85 and Rb 87*, Physical Review **50** (1936) 220.

[18] W. Demtröder, *Experimentalphysik 3 Atome, Molekule Und Festkörper*, Experimentalphysik / Wolfgang Demtröder, Springer Berlin Heidelberg, 2010, ISBN: 9783642039119.

[19] A. Banerjee, D. Das and V. Natarajan, *Precise fine-structure and hyperfine-structure measurements in Rb*, arXiv: Atomic Physics (2002).

[20] B. E. Schultz, H. Ming, G. A. Noble and W. A. van Wijngaarden, *Measurement of the Rb D2 transition linewidth at ultralow temperature*, The European Physical Journal D **48** (2008) 171.

[21] D. W. Preston, *Doppler-free saturated absorption: Laser spectroscopy*, American Journal of Physics **64** (1996) 1432.

[22] V. S. Letokhov, "Saturation spectroscopy", *High-Resolution Laser Spectroscopy*, ed. by S. Amelinkcx et al., vol. 13, Berlin, Heidelberg: Springer Berlin Heidelberg, 1976 95, ISBN: 9783540077190 9783540382379.

[23] U. Schünemann, H. Engler, R. Grimm, M. Weidemüller and M. Zielonkowski, *Simple scheme for tunable frequency offset locking of two lasers*, Review of Scientific Instruments **70** (1999) 242.

Acknowledgements

I would like to thank the entire Nonlinear Quantum Optics group for being so welcoming. I learned a lot during these past months, and I am thankful for this and all the nice lunches and breaks with them.
I want to especially thank Prof. Sebastian Hofferberth for allowing me to write my bachelor thesis in his group and for inspiring me to write my thesis in the field of quantum optics with his great Advanced AMO physics lecture. I would also like to thank Dr. Frank Vewinger for being the second appraiser for this thesis.

A huge thank you to Lukas for the guidance throughout this time and for proofreading my thesis. Your help was vital to the success of my project. I would also like to thank everyone else who proofread my thesis: thank you Nina, Julia and Theresa for all your support! Thank you to Julia for all the fun coffee breaks and for the help when you were actually coming by the lab for something else entirely.

A special thank you to Theresa for being such a great friend, for all the breaks and the advice. I want to thank Kim for being the best lab mate, both helping with any problem and providing fun breaks in between - I will miss working on our theses together.

I also want to thank Tina for being so kind and welcoming and for helping with any questions.

Finally, I want to thank my friends and family for all their support.